G. Stefanucci, S. Kurth, E.K.U. Gross and A. Rubio, Molecular and nano electronics: analysis, design and simulation, J. Seminario, ed(s), Elsevier Series on Theoretical and Computational Chemistry 17, p.247-284 (2007).

Time dependent transport phenomena

G. Stefanucci, S. Kurth, E.K.U. Gross

Institut für Theoretische Physik, Freie Universität Berlin, Arnimallee 14, D-14195 Berlin, Germany, and European Theoretical Sepctroscopy Facility (ETSF)

A. Rubio

Departamento de Física de Materiales, Facultad de Ciencias Químicas, UPV/EHU, Unidad de Materiales Centro Mixto CSIC-UPV/EHU and Donostia International Physics Center (DIPC), San Sebastián, Spain, and European Theoretical Sepctroscopy Facility (ETSF)

1 Introduction

The aim of this review is to give a pedagogical introduction to our recently proposed *ab initio* theory of quantum transport. It is not intended to be a general overview of the field. For further information we refer the interested reader to Refs. [1–3]. The nomenclature *quantum transport* has been coined for the phenomenon of electron motion through constrictions of transverse dimensions smaller than the electron wavelength, e.g., quantum-point contacts, quantum wires, molecules, etc. The typical experimental setup is displayed in Fig. 1 where a central region C of meso- or nano-scopic size is coupled to two metallic electrodes L and R which play the role of charge reservoirs. The whole system is initially (at time $t < 0$) in a well defined equilibrium configuration, described by a *unique* temperature and chemical potential (thermodynamic consistency). The charge density of the electrodes is perfectly balanced and no current flows through the junction.

As originally proposed by Cini [4], we may drive the system out of equilibrium by exposing the electrons to an external time-dependent potential which is local in time and space. For instance, we may switch on an electric field by putting the system between two capacitor plates far away from the system boundaries. The dynamical formation of dipole layers screens the potential drop along the electrodes and the total potential turns out to be uniform in the left and right bulks. Accordingly, the potential drop is entirely limited to the central region. As the system size increases, the remote parts are less

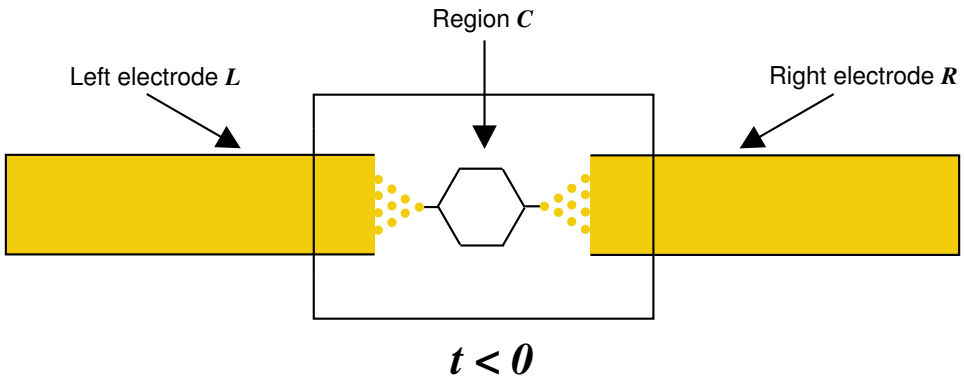

Fig. 1. Schematic sketch of the experimental setup described in the main text. A central region which also includes few layers of the left and right electrodes is coupled to macroscopically large metallic reservoirs. The system is in equilibrium for negative times.

disturbed by the junction, and the density inside the electrodes approaches the equilibrium bulk density.

The Cini scheme can be combined with Time Dependent Density Functional Theory (TDDFT).[5] In this theory, the time-dependent density of an interacting system moving in an external, time-dependent local potential can be calculated via a fictitious system of non-interacting electrons moving in a local, effective time-dependent potential. Therefore this theory is in principle well suited for the treatment of nonequilibrium transport problems.[6] However, as far as the leads are treated as *noninteracting*, it is not obvious that in the long-time limit a steady-state current can ever develop. The reason behind the uncertainty is that the bias represents a large perturbation and, in the absence of dissipative effects, e.g., electron-electron or electron-phonon scattering, the return of time-translational invariance is not granted. In this review we will show that the total current tends to a steady-state value provided the effective potential of TDDFT is independent of time and space in the left and right bulks. Also, the physical mechanism leading to the dynamical formation of a steady state is clarified.

It should be mentioned that there has been already considerable activity in the density functional theory (DFT) community to describe transport phenomena through systems like the one in Fig. 1. Most approaches are limited to the steady-state regime and are based on a self-consistency procedure first proposed by Lang.[7] In this steady-state approach based on DFT, exchange and correlation is approximated by the static Kohn-Sham (KS) potential and the charge density is obtained self-consistently in the presence of the steady current. However, the original justification involved subtle points such as different Fermi levels deep inside the left and right electrodes (which is not thermodynamically consistent) and the implicit reference of non-local perturbations such as tunneling Hamiltonians within a DFT framework. (For a

detailed discussion we refer to Ref. [8].) Furthermore, the transmission functions computed from static DFT have resonances at the non-interacting KS excitation energies which in general do not coincide with the true excitation energies.

Our TDDFT formulation, as opposed to the static DFT formulation, is thermodynamically consistent, is not limited to the steady-state regime (we can study transients, AC responses, etc.) and has the extra merit of accessing the true excitation energies of interacting systems.[9]

We will first use the nonequilibrium Green's function (NEGF) technique to discuss the implications of our approach. For those readers that are not familiar with the Keldysh formalism and with NEGF, in Section 2 we give an elementary introduction to the Keldysh contour, the Keldysh-Green functions and the Keldysh book-keeping. The aim of this Section is to derive some of the identities needed for the discussion (thus providing a self-contained presentation) and to establish the basic notation. In Section 3 we set up the theoretical framework by combining TDDFT and NEGF. An exact expression for the time-dependent total current $I(t)$ is written in terms of Green functions projected in region C. It is also shown that a steady-state regime develops provided 1) the KS Hamiltonian *globally* converges to an asymptotic KS Hamiltonian when $t \to \infty$, 2) the electrodes form a continuum of states (thermodynamic limit), and 3) the local density of states is a smooth function in the central region. It is worth noting that the steady-state current results from a pure dephasing mechanism in the fictitious KS system. Also, the resulting steady current only depends on the KS potential at $t = \infty$ and not on its history. However, the KS potential might depend on the history of the external applied potential and the resulting steady-state current might be history dependent. A practical scheme to calculate $I(t)$ is presented in Section 4. The main idea is to propagate the KS orbitals in region C only, without dealing with the infinite and non-periodic system.[10] We first show how to obtain the KS eigenstates ψ_s of the undisturbed system in Section 4.1. Then, in Section 4.2 we describe an algorithm for propagating ψ_s under the influence of a time-dependent disturbance. The numerical approach of Section 4 is completely general and can be applied to any system having the geometry sketched in Fig. 1. In order to demonstrate the feasibility of the scheme we implement it for one-dimensional model systems in Section 5. Here we study the dynamical current response of several systems perturbed by DC and AC biases. We verify that for noninteracting electrons the steady-state current does not depend on the history of the applied bias. Also, we present preliminary results on net currents in unbiased systems as obtained by pumping mechanisms. We summarize our findings and draw our conclusions in Section 6.

2 The Keldysh formalism

2.1 The Keldysh contour

In quantum mechanics we associate to any observable quantity O a hermitian operator $\hat{O}$. The expectation $\langle\Psi|\hat{O}|\Psi\rangle$ gives the value of O when the system is described by the state $|\Psi\rangle$. For an isolated system the Hamiltonian $\hat{H}_0$ does not depend on time, and the expectation value of *any* observable quantity is constant provided $|\Psi\rangle$ is an eigenstate of $\hat{H}_0$. In this Section we discuss how to describe systems which are not isolated but perturbed by external fields. Without loss of generality, we assume that the system is isolated for negative times t and that $\hat{H}(t<0)=\hat{H}_0$. The evolution of the state $|\Psi\rangle$ is governed by the Schrödinger equation $i\frac{\mathrm{d}}{\mathrm{d}t}|\Psi(t)\rangle=\hat{H}(t)|\Psi(t)\rangle$, and, correspondingly, the value of O evolves in time as $O(t)=\langle\Psi(t)|\hat{O}|\Psi(t)\rangle$. The time-evolved state $|\Psi(t)\rangle=\hat{S}(t;0)|\Psi(0)\rangle$, where the evolution operator $\hat{S}(t;t')$ can be formally written as

$$\hat{S}(t;t')=\begin{cases} T\,\mathrm{e}^{-i\int_{t'}^{t}\mathrm{d}\bar{t}\,\hat{H}(\bar{t})} & t>t' \\ \overline{T}\,\mathrm{e}^{-i\int_{t'}^{t}\mathrm{d}\bar{t}\,\hat{H}(\bar{t})} & t<t' \end{cases}. \tag{1}$$

In Eq. (1), T is the time-ordering operator and rearranges the operators in chronological order with later times to the left; $\overline{T}$ is the anti-chronological time-ordering operator. The evolution operator is unitary and satisfies the group property $\hat{S}(t;t_1)\hat{S}(t_1;t')=\hat{S}(t;t')$ for any t_1. It follows that $O(t)$ is the average on the initial state $|\Psi(0)\rangle$ of the operator $\hat{O}$ in the Heisenberg representation, $\hat{O}_H(t)=\hat{S}(0;t)\hat{O}\hat{S}(t;0)$, i.e.,

$$\begin{aligned} O(t)&=\langle\Psi(0)|\hat{S}(0;t)\hat{O}\hat{S}(t;0)|\Psi(0)\rangle \\ &=\langle\Psi(0)|\overline{T}\mathrm{e}^{-i\int_{t}^{0}\mathrm{d}\bar{t}\,\hat{H}(\bar{t})}\;\hat{O}\;T\mathrm{e}^{-i\int_{0}^{t}\mathrm{d}\bar{t}\,\hat{H}(\bar{t})}|\Psi(0)\rangle. \end{aligned} \tag{2}$$

We can now design an oriented contour γ with a forward branch going from $t=0$ to t and a backward branch coming back from t and ending in $t=0$, see Fig. 2.a. Denoting with $\bar{z}$ the variable running on γ, Eq. (2) can be formally recast as follows

$$O(t)=\langle\Psi(0)|T_{\mathrm{K}}\left\{\mathrm{e}^{-i\int_{\gamma}\mathrm{d}\bar{z}\,\hat{H}(\bar{z})}\;\hat{O}(t)\right\}|\Psi(0)\rangle. \tag{3}$$

The contour ordering operator T_{K} moves the operators with "later" contour variable to the left. A point z is later than a point z' if z' is closer to the starting point, see Fig. 2.a. In Eq. (3), $\hat{O}(t)$ is *not* the operator in the Heisenberg representation [the latter is denoted with $\hat{O}_H(t)$]. Actually, $\hat{O}(t)=\hat{O}$ for any

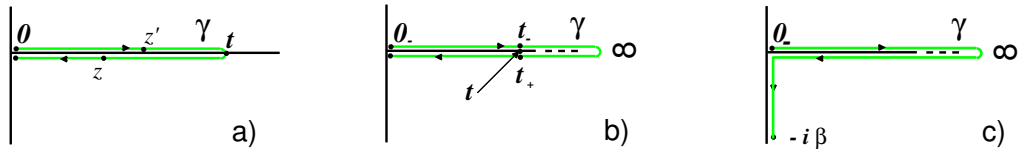

Fig. 2. a) The oriented contour γ described in the main text with a forward and a backward branch between 0 and t. According with the orientation the point z is later than the point z'. b) The extended oriented contour γ described in the main text with a forward and a backward branch between 0 and ∞. For any physical time t we have two points $t_\pm$ on γ at the same distance from the origin. c) The generalization of the original Keldysh contour. A vertical track going from 0 to $-i\beta$ has been added and, according with the orientation chosen, any point lying on it is later than a point lying on the forward or backward branch.

t. The reason of the time argument stems from the need of specifying the position of the operator $\hat{O}$ in the contour ordering.

Let us now extend the contour γ up to infinity, as shown in Fig. 2.b. For any physical time t there are two points $z = t_+$ and $z = t_-$ on γ; t_- lies on the forward branch while t_+ lies on the backward branch and it is later than t_- according with the orientation chosen. We have $T_{\rm K}\{{\rm e}^{-i\int_\gamma {\rm d}\bar{z}\,\hat{H}(\bar{z})}\ \hat{O}(t_-)\} = \hat{S}(0;\infty)\hat{S}(\infty;t)\hat{O}(t)\hat{S}(t;0) = \hat{S}(0;t)\hat{O}\hat{S}(t;0)$, and similarly $T_{\rm K}\{{\rm e}^{-i\int_\gamma {\rm d}\bar{z}\,\hat{H}(\bar{z})}\ \hat{O}(t_+)\} = \hat{S}(0;t)\hat{O}(t)\hat{S}(t;\infty)\hat{S}(\infty;0) = \hat{S}(0;t)\hat{O}\hat{S}(t;0)$. Thus, the expectation value $O(t)$ in Eq. (3) is also given by the formula

$$O(z) = \langle\Psi(0)|T_{\rm K}\left\{{\rm e}^{-i\int_\gamma {\rm d}\bar{z}\,\hat{H}(\bar{z})}\ \hat{O}(z)\right\}|\Psi(0)\rangle. \qquad (4)$$

where γ is the contour in Fig. 2.b; γ is called the *Keldysh contour*.[11,12] In Eq. (4) the variable z can be either t_- or t_+ and $O(t_-) = O(t_+) = O(t)$.

The Keldysh contour can be further extended to account for statistical averages.[13] In statistical physics a system is described by the density matrix $\hat{\rho} = \sum_n w_n|\Psi_n\rangle\langle\Psi_n|$ with w_n the probability of finding the system in the state $|\Psi_n\rangle$ and $\sum_n w_n = 1$. The states $|\Psi_n\rangle$ may not be orthogonal. We say that the system is in a pure state if $\hat{\rho} = |\Psi\rangle\langle\Psi|$. In a system described by a density matrix $\hat{\rho}(0)$ at $t = 0$, the time-dependent value of the observable O is a generalization of Eq. (4), i.e., $O(z) = \sum_n w_n\langle\Psi_n(0)|T_{\rm K}\{{\rm e}^{-i\int_\gamma {\rm d}\bar{z}\,\hat{H}(\bar{z})}\ \hat{O}(z)\}|\Psi_n(0)\rangle$. Among all possible density matrices there is one that is very common in physics and describes a system in thermal equilibrium: $\hat{\rho} = \exp[-\beta(\hat{H}_0 - \mu\hat{N})]/\mathcal{Z}$, with the inverse temperature β, the chemical potential μ, the operator $\hat{N}$ corresponding to the total number of particles and the grand-partition function $\mathcal{Z} = {\rm Tr}\exp[-\beta(\hat{H}_0 - \mu\hat{N})]$. Assuming that $\hat{H}_0$ and $\hat{N}$ commute, the statistical average $O(z)$ with the thermal density matrix can be written as $O(z) = {\rm Tr}\,[\,{\rm e}^{\beta\mu\hat{N}}{\rm e}^{-\beta\hat{H}_0}T_{\rm K}\{{\rm e}^{-i\int_\gamma {\rm d}\bar{z}\,\hat{H}(\bar{z})}\ \hat{O}(z)\}\,]/\mathcal{Z}$. We can now extend further the Keldysh contour as shown in Fig. 2.c and define $\hat{H}(z) = \hat{H}_0$ for any z

on the vertical track. With this definition $\hat{H}(z)$ is continuous along the entire contour since $\hat{H}(0) = \hat{H}_0$. According to the orientation displayed in the figure, any point lying on the vertical track is later than a point lying on the forward or backward branch. We use this observation to rewrite $O(z)$ as

$$O(z) = \frac{\mathrm{Tr}\,\left[\mathrm{e}^{\beta\mu\hat{N}} T_{\mathrm{K}} \left\{ \mathrm{e}^{-i\int_\gamma \mathrm{d}\bar{z}\,\hat{H}(\bar{z})}\,\hat{O}(z) \right\}\right]}{\mathrm{Tr}\,\left[\mathrm{e}^{\beta\mu\hat{N}} T_{\mathrm{K}} \left\{ \mathrm{e}^{-i\int_\gamma \mathrm{d}\bar{z}\,\hat{H}(\bar{z})} \right\}\right]}, \tag{5}$$

where T_{K} is now the ordering operator on the extended contour. It is worth noting that the denominator in the above expression is simply $\mathcal{Z}$. We have already shown that choosing z on one of the two horizontal branches, Eq. (5) yields the time-dependent statistical average of the observable O. On the other hand, if z lies on the vertical track $O(z) = \mathrm{Tr}\,[\,\mathrm{e}^{\beta\mu\hat{N}} \mathrm{e}^{-i\int_z^{-i\beta} \hat{H}_0} \hat{O} \mathrm{e}^{-i\int_0^z \hat{H}_0}\,]/\mathcal{Z} = \mathrm{Tr}\,[\,\mathrm{e}^{-\beta(\hat{H}_0-\mu\hat{N})}\hat{O}]/\mathcal{Z}$, where the cyclic property of the trace has been used. The result is independent of z and coincides with the thermal average of the observable O.

To summarize, in Eq. (5) the variable z lies on the contour of Fig. 2.c; the r.h.s. gives the time-dependent statistical average of the observable quantity O when z lies on the forward or backward branch, and the statistical average before the system is disturbed when z lies on the vertical track.

2.2 The Keldysh-Green function

The idea presented in the previous Section can be used to define correlators of many operators on the extended Keldysh contour. The Keldysh-Green function $\boldsymbol{G}$ is the correlator of two field operators $\psi(\boldsymbol{r})$ and $\psi^\dagger(\boldsymbol{r})$ which obey the anticommutation relations $\{\psi(\boldsymbol{r}), \psi^\dagger(\boldsymbol{r}')\} = \delta(\boldsymbol{r} - \boldsymbol{r}')$. It is defined as

$$\langle \boldsymbol{r}|\boldsymbol{G}(z;z')|\boldsymbol{r}'\rangle = \frac{1}{i}\frac{\mathrm{Tr}\,\left[\mathrm{e}^{\beta\mu\hat{N}} T_{\mathrm{K}} \left\{ \mathrm{e}^{-i\int_\gamma \mathrm{d}\bar{z}\,\hat{H}(\bar{z})}\,\psi(\boldsymbol{r},z)\psi^\dagger(\boldsymbol{r}',z') \right\}\right]}{\mathrm{Tr}\,\left[\mathrm{e}^{\beta\mu\hat{N}} T_{\mathrm{K}} \left\{ \mathrm{e}^{-i\int_\gamma \mathrm{d}\bar{z}\,\hat{H}(\bar{z})} \right\}\right]}, \tag{6}$$

where the contour variable in the field operators specifies the position in the contour ordering (there is no true dependence on z in ψ and $\psi^\dagger$). Here and in the following we use boldface to indicate matrices in one-electron labels, *e.g.*, $\boldsymbol{G}$ is a matrix and $\langle \boldsymbol{r}|\boldsymbol{G}|\boldsymbol{r}'\rangle$ is the $(\boldsymbol{r},\boldsymbol{r}')$ matrix element of $\boldsymbol{G}$. Due to the contour ordering operator T_{K}, the Green function $\boldsymbol{G}$ has the following structure

$$\boldsymbol{G}(z;z') = \theta(z,z')\boldsymbol{G}^{>}(z;z') + \theta(z',z)\boldsymbol{G}^{<}(z;z'), \tag{7}$$

where $\theta(z,z') = 1$ if z is later than z' on the contour and zero otherwise. We say that a two-point function on the contour having the above structure belongs

to the *Keldysh space*. The Green function $\boldsymbol{G}(z;z')$ obeys an important cyclic relation on the extended Keldysh contour. As we shall see, the relations below play a crucial role since they provide the boundary conditions for solving the Dyson equation. Choosing $z = 0_-$ we find

$$\langle \boldsymbol{r}|\boldsymbol{G}(0_-;z')|\boldsymbol{r}'\rangle = -\frac{1}{i}\frac{\mathrm{Tr}\left[\mathrm{e}^{\beta\mu\hat{N}}T_{\mathrm{K}}\left\{\mathrm{e}^{-i\int_\gamma \mathrm{d}\bar{z}\,\hat{H}(\bar{z})}\psi^\dagger(\boldsymbol{r}',z')\right\}\psi(\boldsymbol{r})\right]}{\mathrm{Tr}\left[\mathrm{e}^{\beta\mu\hat{N}}T_{\mathrm{K}}\left\{\mathrm{e}^{-i\int_\gamma \mathrm{d}\bar{z}\,\hat{H}(\bar{z})}\right\}\right]}, \qquad (8)$$

where we have taken into account that 0_- is the earliest time and therefore $\psi(\boldsymbol{r},0_-)$ is always moved to the right when acted upon by T_{K}. The extra minus sign in the r.h.s. comes from the contour ordering. More generally, rearranging the field operators ψ and $\psi^\dagger$ (later arguments to the left), we also have to multiply by $(-1)^P$, where P is the parity of the permutation. Inside the trace we can move $\psi(\boldsymbol{r})$ to the left. Furthermore, we can exchange the position of $\psi(\boldsymbol{r})$ and $\mathrm{e}^{\beta\mu\hat{N}}$ by noting that $\psi(\boldsymbol{r})\mathrm{e}^{\beta\mu\hat{N}} = \mathrm{e}^{\beta\mu(\hat{N}+1)}\psi(\boldsymbol{r})$. Using the fact that T_{K} moves operators with later times to the left we have $\psi(\boldsymbol{r})T_{\mathrm{K}}\{\ldots\} = T_{\mathrm{K}}\{\psi(\boldsymbol{r},-i\beta)\ldots\}$. Therefore, we conclude that

$$\boldsymbol{G}(0_-;z') = -\mathrm{e}^{\beta\mu}\boldsymbol{G}(-i\beta;z'), \qquad \boldsymbol{G}(z;0_-) = -\mathrm{e}^{-\beta\mu}\boldsymbol{G}(z;-i\beta), \qquad (9)$$

where the second of these relations can be obtained in a similar way. Eq. (9) are the so called Kubo-Martin-Schwinger (KMS) boundary conditions.[14,15]

2.3 The Keldysh book-keeping

In this Section we derive some of the identities that we will use for dealing with time-dependent transport phenomena. A systematic and more exhaustive discussion can be found in Ref. [16].

Let $k(z;z')$ belong to the Keldysh space: $k(z;z') = \theta(z,z')k^{>}(z;z') + \theta(z',z)k^{<}(z;z')$. For any $k(z;z')$ in the Keldysh space we define the *greater* and *lesser* functions on the physical time axis

$$k^{>}(t;t') \equiv k(t_+;t'_-), \quad k^{<}(t,t') \equiv k(t_-;t'_+). \qquad (10)$$

We also define the *left* and *right* functions with one argument t on the physical time axis and the other τ on the vertical track

$$k^{\rceil}(t;\tau) \equiv k(t_\pm;\tau), \quad k^{\lceil}(\tau,t) \equiv k(\tau;t_\pm). \qquad (11)$$

In the definition of $k^{\rceil}$ and $k^{\lceil}$ we can arbitrarily choose t_+ or t_- since τ is later than both of them. The symbols "$\rceil$" and "$\lceil$" have been chosen in order to help the visualization of the time arguments. For instance, "$\rceil$" has a horizontal

segment followed by a vertical one; correspondingly, $k^{\rceil}$ has a first argument which is real (and thus lies on the horizontal axis) and a second argument which is imaginary (and thus lies on the vertical axis). We will also use the convention of denoting with Latin letters the real time and with Greek letters the imaginary time.

It is straightforward to show that if $a(z;z')$ and $b(z;z')$ belong to the Keldysh space, then $c(z;z') = \int_\gamma \mathrm{d}\bar{z}\ a(z;\bar{z})b(\bar{z};z')$ also belongs to the Keldysh space. From the definitions (10-11) we find

$$\begin{aligned} c^{>}(t;t') = & \int_{0_-}^{t'_-} \mathrm{d}\bar{z}\ a^{>}(t_+;\bar{z})b^{<}(\bar{z};t'_-) + \int_{t'_-}^{t_+} \mathrm{d}\bar{z}\ a^{>}(t_+;\bar{z})b^{>}(\bar{z};t'_-) \\ & + \int_{t_+}^{-i\beta} \mathrm{d}\bar{z}\ a^{<}(t_+;\bar{z})b^{>}(\bar{z};t'_-) = \\ & = \int_0^{t'} \mathrm{d}\bar{t}\ a^{>}(t;\bar{t})b^{<}(\bar{t};t') + \int_{t'}^{t} \mathrm{d}\bar{t}\ a^{>}(t;\bar{t})b^{>}(\bar{t};t') \\ & + \int_t^0 \mathrm{d}\bar{t}\ a^{<}(t;\bar{t})b^{>}(\bar{t};t') + \int_0^{-i\beta} \mathrm{d}\bar{\tau}\ a^{\rceil}(t;\bar{\tau})b^{\lceil}(\bar{\tau};t'). \end{aligned} \tag{12}$$

The second integral on the r.h.s. is an ordinary integral on the real axis of two well defined functions and may be rewritten as $\int_{t'}^{t} \mathrm{d}\bar{t}\ a^{>}(t;\bar{t})b^{>}(\bar{t};t') = \int_{t'}^{0} \mathrm{d}\bar{t}\ a^{>}(t;\bar{t})b^{>}(\bar{t};t') + \int_0^t \mathrm{d}\bar{t}\ a^{>}(t;\bar{t})b^{>}(\bar{t};t')$. Using this relation, Eq. (12) becomes

$$c^{>}(t;t') = \int_0^\infty \mathrm{d}\bar{t}\ [a^{>}(t;\bar{t})b^{\mathrm{A}}(\bar{t};t') + a^{\mathrm{R}}(t;\bar{t})b^{>}(\bar{t};t')] + \int_0^{-i\beta} \mathrm{d}\bar{\tau}\ a^{\rceil}(t;\bar{\tau})b^{\lceil}(\bar{\tau};t'), \tag{13}$$

where we have introduced two other functions on the physical time axis

$$k^{\mathrm{R}}(t;t') \equiv \theta(t-t')[k^{>}(t;t') - k^{<}(t;t')],$$

$$k^{\mathrm{A}}(t;t') \equiv -\theta(t'-t)[k^{>}(t;t') - k^{<}(t;t')]. \tag{14}$$

The *retarded* function $k^{\mathrm{R}}(t;t')$ vanishes for $t < t'$, while the *advanced* function $k^{\mathrm{A}}(t;t')$ vanishes for $t > t'$. A relation similar to Eq. (13) can be obtained for the lesser component $c^{<}$. It is convenient to introduce a shorthand notation for integrals along the physical time axis and for those between 0 and $-i\beta$. The symbol "$\cdot$" will be used to write $\int_0^\infty \mathrm{d}\bar{t} f(\bar{t})g(\bar{t})$ as $f \cdot g$, while the symbol "$\star$" will be used to write $\int_0^{-i\beta} \mathrm{d}\bar{\tau} f(\bar{\tau})g(\bar{\tau})$ as $f \star g$. Then

$$c^{>} = a^{>} \cdot b^{\mathrm{A}} + a^{\mathrm{R}} \cdot b^{>} + a^{\rceil} \star b^{\lceil}, \qquad c^{<} = a^{<} \cdot b^{\mathrm{A}} + a^{\mathrm{R}} \cdot b^{<} + a^{\rceil} \star b^{\lceil}. \tag{15}$$

Eq. (15) can be used to extract the retarded and advanced component of c. By definition $c^{\mathrm{R}}(t;t') = \theta(t-t')[c^{>}(t;t') - c^{<}(t;t')]$ and therefore

$$c^{\mathrm{R}}(t;t') = \theta(t-t')\int_0^\infty \mathrm{d}\bar{t}\, a^{\mathrm{R}}(t;\bar{t})[b^{>}(\bar{t};t') - b^{<}(\bar{t};t')] + \theta(t-t')\int_0^\infty \mathrm{d}\bar{t}\,[a^{>}(t;\bar{t}) - a^{<}(t;\bar{t})]b^{\mathrm{A}}(\bar{t};t'). \quad (16)$$

Due to the θ-function, we have $t > t'$ for $c^{\mathrm{R}} \neq 0$. In the second term on the r.h.s. $b^{\mathrm{A}}(\bar{t};t')$ contains a $\theta(t'-\bar{t})$ and hence it must be $t > \bar{t}$; therefore we can replace the difference in the square bracket with a^{R}. Then we break the first term on the r.h.s. in two pieces by inserting θ-functions: one for $\bar{t} < t'$ and the other for $\bar{t} > t'$. In compact notation we end up with

$$c^{\mathrm{R}} = a^{\mathrm{R}} \cdot b^{\mathrm{R}}, \qquad c^{\mathrm{A}} = a^{\mathrm{A}} \cdot b^{\mathrm{A}}, \quad (17)$$

where the second relation can be proven in a similar way. It is worth noting that in the expressions for c^{R} and c^{A} no integration along the imaginary track is required. For later purposes we also define the *Matsubara* function $k^{\mathrm{M}}(\tau;\tau')$ with both the arguments in the interval $(0, -i\beta)$:

$$k^{\mathrm{M}}(\tau;\tau') \equiv k(z=\tau; z'=\tau'). \quad (18)$$

It is straightforward to prove the following identities

$$c^{\rceil} = a^{\mathrm{R}} \cdot b^{\rceil} + a^{\rceil} \star b^{\mathrm{M}}, \qquad c^{\lceil} = a^{\lceil} \cdot b^{\mathrm{A}} + a^{\mathrm{M}} \star b^{\lceil}, \qquad c^{\mathrm{M}} = a^{\mathrm{M}} \star b^{\mathrm{M}}. \quad (19)$$

Finally, we consider the case of a Keldysh function $k(z;z')$ multiplied on the left by a scalar function $l(z)$. The function $k_l(z;z') = l(z)k(z;z') = \theta(z,z')l(z)k^{>}(z;z') + \theta(z';z)l(z)k^{<}(z;z')$ and hence belongs to the Keldysh space. The Keldysh components can be extracted using the definitions (10,11,14,18). Choosing for instance $z = t_+$ and $z' = t'_-$ we find $k_l^{>}(t;t') = l(t)k^{>}(t;t')$ and similarly for $z = t_-$ and $z' = t'_+$ we find $k_l^{<}(t;t') = l(t)k^{<}(t;t')$. More generally, the function l is simply a prefactor: $k_l^{\mathrm{x}} = lk^{\mathrm{x}}$, where x is one of the Keldysh components ($\lessgtr$, R, A, $\rceil$, $\lceil$, M). The same is true for $k_r(z;z') = k(z;z')r(z')$, where $r(z')$ is a scalar function: $k_r^{\mathrm{x}} = k^{\mathrm{x}}r$.

3 Quantum transport using TDDFT and NEGF

3.1 Merging the Keldysh and TDDFT formalisms

The one-particle scheme of TDDFT corresponds to a fictitious system of non-interacting electrons described by the Kohn-Sham (KS) Hamiltonian $\hat{H}_s(z) = \int \mathrm{d}\boldsymbol{r}\mathrm{d}\boldsymbol{r}'\psi^\dagger(\boldsymbol{r})\langle\boldsymbol{r}|\boldsymbol{H}_s(z)|\boldsymbol{r}'\rangle\psi(\boldsymbol{r}')$. The potential $v_s(\mathbf{r},t)$ experienced by the electrons in the free-electron Hamiltonian $\boldsymbol{H}_s(t)$ is called the KS potential and it is given by the sum of the external potential, the Coulomb potential of the

nuclei, the Hartree potential and the exchange-correlation potential $v_{\rm xc}$. The latter accounts for the complicated many-body effects and is obtained from an exchange-correlation action functional, $v_{\rm xc}(\mathbf{r},t)=\delta A_{\rm xc}[n]/\delta n(\mathbf{r},t)$ (as pointed out in Ref. [17], the causality and symmetry properties require that the action functional $A_{\rm xc}[n]$ is defined on the Keldysh contour). $A_{\rm xc}$ is a functional of the density and of the initial density matrix. In our case, the initial density matrix is the thermal density matrix which, due to the extension of the Hohenberg-Kohn theorem[18] to finite temperatures,[19] also is a functional of the density. We should mention here that an alternative formulation based on TDDFT has been recently proposed by Di Ventra and Todorov[20]. In their approach the system is initially unbalanced and therefore the exchange-correlation functional depends on the initial state and not only on the density.

The fictitious Keldysh-Green function $\boldsymbol{\mathcal{G}}(z;z')$ of the KS system satisfies a one-particle equation of motion

$$\left\{i\frac{\overrightarrow{\mathrm{d}}}{\mathrm{d}z}\mathbf{1}-\boldsymbol{H}_s(z)\right\}\boldsymbol{\mathcal{G}}(z;z')=\mathbf{1}\delta(z-z'),$$

$$\boldsymbol{\mathcal{G}}(z;z')\left\{-i\frac{\overleftarrow{\mathrm{d}}}{\mathrm{d}z'}\mathbf{1}-\boldsymbol{H}_s(z')\right\}=\mathbf{1}\delta(z-z'), \tag{20}$$

with KMS boundary conditions (9). In Eqs. (20) the arrow specifies where the derivative along the contour acts. The left and right equations of motion are equations on the extended Keldysh contour of Fig. 2.c and $\delta(z-z')=\frac{\mathrm{d}}{\mathrm{d}z}\theta(z,z')=-\frac{\mathrm{d}}{\mathrm{d}z'}\theta(z,z')$. For any $z\neq z'$, the equations of motion are solved by the evolution operator on the contour $\boldsymbol{S}(z;z')=T_{\rm K}\{\mathrm{e}^{-i\int_{z'}^{z}\mathrm{d}\bar{z}\boldsymbol{H}_s(\bar{z})}\}$, since $i\frac{\overrightarrow{\mathrm{d}}}{\mathrm{d}z}\boldsymbol{S}(z;z')=\boldsymbol{H}_s(z)\boldsymbol{S}(z;z')$ and $\boldsymbol{S}(z;z')(-i\frac{\overleftarrow{\mathrm{d}}}{\mathrm{d}z'})=\boldsymbol{S}(z;z')\boldsymbol{H}_s(z')$. Therefore, any Green function

$$\boldsymbol{\mathcal{G}}(z;z')=\theta(z,z')\boldsymbol{S}(z;0_-)\boldsymbol{f}^{>}\boldsymbol{S}(0_-;z')+\theta(z',z)\boldsymbol{S}(z;0_-)\boldsymbol{f}^{<}\boldsymbol{S}(0_-;z'), \tag{21}$$

with $\boldsymbol{f}^{\lessgtr}$ constrained by $\boldsymbol{f}^{>}-\boldsymbol{f}^{<}=-i\mathbf{1}$, is solution of Eqs. (20). In order to fix the matrix $\boldsymbol{f}^{>}$ or $\boldsymbol{f}^{<}$ we impose the KMS boundary conditions. The matrix $\boldsymbol{H}_s(z)=\boldsymbol{H}_s$ for any z on the vertical track, meaning that $\boldsymbol{S}(-i\beta;0_-)=\mathrm{e}^{-\beta\boldsymbol{H}_s}$. Eq. (9) then implies $\boldsymbol{f}^{<}=-\mathrm{e}^{-\beta(\boldsymbol{H}_s-\mu)}\boldsymbol{f}^{>}$, and taking into account the constraint $\boldsymbol{f}^{>}-\boldsymbol{f}^{<}=-i\mathbf{1}$ we conclude that $\boldsymbol{f}^{<}=if(\boldsymbol{H}_s)$, where $f(\omega)=1/[\mathrm{e}^{\beta(\omega-\mu)}+1]$ is the Fermi distribution function. The matrix $\boldsymbol{f}^{>}$ takes the form $\boldsymbol{f}^{>}=i[f(\boldsymbol{H}_s)-\mathbf{1}]$.

The Green function $\boldsymbol{\mathcal{G}}(z;z')$ for a system of non-interacting electrons is now completely fixed. Let us consider some Keldysh-Green functions. For $z=t_+$ and $z'=t_-$ we have the *greater* Green function while for $z=t_-$ and $z'=t_+$

we have the *lesser* Green function

$$\boldsymbol{\mathcal{G}}^{>}(t;t') = i\,\boldsymbol{S}(t;0)[f(\boldsymbol{H}_s) - \mathbf{1}]\boldsymbol{S}(0;t'), \quad \boldsymbol{\mathcal{G}}^{<}(t;t') = i\,\boldsymbol{S}(t;0)f(\boldsymbol{H}_s)\boldsymbol{S}(0;t'). \tag{22}$$

Both $\boldsymbol{\mathcal{G}}^{>}$ and $\boldsymbol{\mathcal{G}}^{<}$ depend on the initial distribution function $f(\boldsymbol{H}_s)$. The diagonal matrix element of $-i\boldsymbol{\mathcal{G}}^{<}$ is nothing but the time-dependent value of the local electron density $n(\boldsymbol{r},t)$, while $i\boldsymbol{\mathcal{G}}^{>}$ gives the local density of holes. Another way of writing $-i\boldsymbol{\mathcal{G}}^{<}$ is in terms of the eigenstates $|\psi_s(0)\rangle$ of $\boldsymbol{H}_s$ with eigenvalues ε_s. From the time-evolved eigenstate $|\psi_s(t)\rangle = \boldsymbol{S}(t;0)|\psi_s(0)\rangle$ we can calculate the time-dependent wavefunction $\psi_s(\boldsymbol{r},t) = \langle\boldsymbol{r}|\psi_s(t)\rangle$. Inserting $\sum_s |\psi_s(0)\rangle\langle\psi_s(0)|$ in the expression for $\boldsymbol{\mathcal{G}}^{<}$ we find $-i\langle\boldsymbol{r}|\boldsymbol{\mathcal{G}}^{<}(t;t')|\boldsymbol{r}'\rangle = \sum_s f(\varepsilon_s)\psi_s(\boldsymbol{r},t)\psi_s^*(\boldsymbol{r}',t')$, which for $t = t'$ reduces to the time-dependent density matrix. Knowing the greater and lesser Green functions we can also calculate $\boldsymbol{\mathcal{G}}^{\mathrm{R,A}}$. Taking into account the definitions (14) we find

$$\boldsymbol{\mathcal{G}}^{\mathrm{R}}(t;t') = -i\theta(t-t')\boldsymbol{S}(t;t'), \quad \boldsymbol{\mathcal{G}}^{\mathrm{A}}(t;t') = i\theta(t'-t)\boldsymbol{S}(t;t') = [\boldsymbol{\mathcal{G}}^{\mathrm{R}}(t';t)]^{\dagger}. \tag{23}$$

In the above expressions for $\boldsymbol{\mathcal{G}}^{\mathrm{R,A}}$ the Fermi distribution function has disappeared. The information carried by $\boldsymbol{\mathcal{G}}^{\mathrm{R,A}}$ is the same contained in the one-particle evolution operator. There is no information on how the system is prepared (how many particles, how they are distributed, etc). We use this observation to rewrite $\boldsymbol{\mathcal{G}}^{\lessgtr}$ in terms of $\boldsymbol{\mathcal{G}}^{\mathrm{R,A}}$

$$\boldsymbol{\mathcal{G}}^{\lessgtr}(t;t') = \boldsymbol{\mathcal{G}}^{\mathrm{R}}(t;0)\boldsymbol{\mathcal{G}}^{\lessgtr}(0;0)\boldsymbol{\mathcal{G}}^{\mathrm{R}}(0;t'). \tag{24}$$

Thus, $\boldsymbol{\mathcal{G}}^{\lessgtr}$ is completely known once we know how to propagate the one-electron orbitals in time and how they are populated before the system is perturbed.[4,21] For later purposes, we also observe that an analogous relation holds for $\boldsymbol{\mathcal{G}}^{\rceil,\lceil}$

$$\boldsymbol{\mathcal{G}}^{\rceil}(t;\tau) = i\boldsymbol{\mathcal{G}}^{\mathrm{R}}(t;0)\boldsymbol{\mathcal{G}}^{\rceil}(0;\tau), \quad \boldsymbol{\mathcal{G}}^{\lceil}(\tau;t) = -i\boldsymbol{\mathcal{G}}^{\lceil}(\tau;0)\boldsymbol{\mathcal{G}}^{\mathrm{A}}(0;t). \tag{25}$$

3.2 Total current using TDDFT

The fictitious $\boldsymbol{\mathcal{G}}$ of the KS system will in general not give correct one-particle properties. However by definition $\boldsymbol{\mathcal{G}}^{<}$ gives the correct density $n(\boldsymbol{r},t) = -i\langle\boldsymbol{r}|\boldsymbol{\mathcal{G}}^{<}(t;t)|\boldsymbol{r}\rangle$. Also total currents are correctly given by TDDFT. If for instance I_α is the total current from a particular region α we have

$$I_\alpha(t) = -e\int_\alpha \mathrm{d}\boldsymbol{r}\;\frac{\mathrm{d}}{\mathrm{d}t}n(\boldsymbol{r},t) = e\int_\alpha \mathrm{d}\boldsymbol{r}\;i\frac{\mathrm{d}}{\mathrm{d}t}\langle\boldsymbol{r}|\boldsymbol{\mathcal{G}}^{<}(t;t)|\boldsymbol{r}\rangle. \tag{26}$$

where the space integral extends over the region α (e is the electron charge). We stress here that I_α is the electronic current (the direction of the current coincides with the direction of the electrons).

At this point, it is convenient to partition the system into three main regions: a central region C consisting of the junction and a few atomic layers of the left and right electrodes and two regions L, R which describe the left and right bulk electrodes. According to this partitioning, the KS Hamiltonian $\boldsymbol{H}_s$ can be written as a 3×3 block matrix, and the left equation of motion in (20) reads

$$\left\{ i\frac{\mathrm{d}}{\mathrm{d}z}\mathbf{1} - \begin{bmatrix} \boldsymbol{H}_{LL}(z) & \boldsymbol{H}_{LC} & 0 \\ \boldsymbol{H}_{CL} & \boldsymbol{H}_{CC}(z) & \boldsymbol{H}_{CR} \\ 0 & \boldsymbol{H}_{RC} & \boldsymbol{H}_{RR}(z) \end{bmatrix} \right\} \boldsymbol{\mathcal{G}}(z;z') = \delta(z-z')\mathbf{1}, \tag{27}$$

with

$$\boldsymbol{\mathcal{G}}(z;z') = \begin{bmatrix} \boldsymbol{\mathcal{G}}_{LL}(z;z') & \boldsymbol{\mathcal{G}}_{LC}(z;z') & \boldsymbol{\mathcal{G}}_{LR}(z;z') \\ \boldsymbol{\mathcal{G}}_{CL}(z;z') & \boldsymbol{\mathcal{G}}_{CC}(z;z') & \boldsymbol{\mathcal{G}}_{CR}(z;z') \\ \boldsymbol{\mathcal{G}}_{RL}(z;z') & \boldsymbol{\mathcal{G}}_{RC}(z;z') & \boldsymbol{\mathcal{G}}_{RR}(z;z') \end{bmatrix} \tag{28}$$

(a similar equation is easily obtained for the right equation of motion). Choosing z on the forward branch of the Keldysh contour and z' on the backward branch of the same contour, we obtain a left and right equation for the lesser Green function. These equations can be used to get rid of the time derivative in Eq. (26). We find for $\alpha = L, R$

$$\begin{aligned} I_\alpha(t) &= e\int \mathrm{d}\boldsymbol{r}\ \langle \boldsymbol{r}| i\frac{\mathrm{d}}{\mathrm{d}t}\boldsymbol{\mathcal{G}}^<_{\alpha\alpha}(t;t)|\boldsymbol{r}\rangle \\ &= e\int \mathrm{d}\boldsymbol{r}\ \langle \boldsymbol{r}|\boldsymbol{H}_{\alpha C}\boldsymbol{\mathcal{G}}^<_{C\alpha}(t;t) - \boldsymbol{\mathcal{G}}^<_{\alpha C}(t;t)\boldsymbol{H}_{C\alpha}|\boldsymbol{r}\rangle = 2e\ \mathrm{Re}\left[\mathrm{Tr}_C\ \{\boldsymbol{Q}_\alpha(t)\}\right], \end{aligned} \tag{29}$$

where

$$\begin{aligned} \boldsymbol{Q}_\alpha(t) \equiv \boldsymbol{\mathcal{G}}^<_{C\alpha}(t;t)\boldsymbol{H}_{\alpha C} &= \left[\boldsymbol{\mathcal{G}}^{\mathrm{R}}(t,0)\boldsymbol{\mathcal{G}}^<(0,0)\boldsymbol{\mathcal{G}}^{\mathrm{A}}(0,t)\right]_{C\alpha}\boldsymbol{H}_{\alpha C} \\ &= \boldsymbol{\mathcal{G}}^{\mathrm{R}}_{CC}(t;0)\boldsymbol{\mathcal{G}}^<_{CC}(0;0)\boldsymbol{\mathcal{G}}^{\mathrm{A}}_{C\alpha}(0;t)\boldsymbol{H}_{\alpha C} \\ &+ \sum_{\beta=L,R} \boldsymbol{\mathcal{G}}^{\mathrm{R}}_{C\beta}(t;0)\boldsymbol{\mathcal{G}}^<_{\beta C}(0;0)\boldsymbol{\mathcal{G}}^{\mathrm{A}}_{C\alpha}(0;t)\boldsymbol{H}_{\alpha C} \\ &+ \sum_{\gamma=L,R} \boldsymbol{\mathcal{G}}^{\mathrm{R}}_{CC}(t;0)\boldsymbol{\mathcal{G}}^<_{C\gamma}(0;0)\boldsymbol{\mathcal{G}}^{\mathrm{A}}_{\gamma\alpha}(0;t)\boldsymbol{H}_{\alpha C} \\ &+ \sum_{\beta\gamma=L,R} \boldsymbol{\mathcal{G}}^{\mathrm{R}}_{C\beta}(t;0)\boldsymbol{\mathcal{G}}^<_{\beta\gamma}(0;0)\boldsymbol{\mathcal{G}}^{\mathrm{A}}_{\gamma\alpha}(0;t)\boldsymbol{H}_{\alpha C} \end{aligned} \tag{30}$$

is a one-particle operator in the central region C and Tr_C denotes the trace over a complete set of one-particle states of C. Let us express the quantity $\boldsymbol{Q}_\alpha$ in terms of the Green function $\boldsymbol{\mathcal{G}}_{CC}$ projected in the central region. We introduce

the uncontacted Green function $\boldsymbol{g}$ which obeys Eqs. (20) with $\boldsymbol{H}_{\alpha C} = \boldsymbol{H}_{C\alpha} = 0$,

$$\left\{ i\frac{\mathrm{d}}{\mathrm{d}z}\mathbf{1} - \begin{bmatrix} \boldsymbol{H}_{LL}(z) & 0 & 0 \\ 0 & \boldsymbol{H}_{CC}(z) & 0 \\ 0 & 0 & \boldsymbol{H}_{RR}(z) \end{bmatrix} \right\} \boldsymbol{g}(z;z') = \delta(z-z')\mathbf{1}, \tag{31}$$

where

$$\boldsymbol{g}(z;z') = \begin{bmatrix} \boldsymbol{g}_{LL}(z;z') & 0 & 0 \\ 0 & \boldsymbol{g}_{CC}(z;z') & 0 \\ 0 & 0 & \boldsymbol{g}_{RR}(z;z') \end{bmatrix} \tag{32}$$

and the same KMS boundary conditions as $\boldsymbol{\mathcal{G}}$. The uncontacted $\boldsymbol{g}$ allows us to convert Eqs. (20) into an integral equation which entails the KMS boundary conditions for $\boldsymbol{\mathcal{G}}$

$$\begin{aligned} \boldsymbol{\mathcal{G}}(z;z') &= \boldsymbol{g}(z;z') + \int_\gamma \mathrm{d}\bar{z}\, \boldsymbol{g}(z;\bar{z})\boldsymbol{H}_{\mathrm{off}}\boldsymbol{\mathcal{G}}(\bar{z};z') \\ &= \boldsymbol{g}(z;z') + \int_\gamma \mathrm{d}\bar{z}\, \boldsymbol{\mathcal{G}}(z;\bar{z})\boldsymbol{H}_{\mathrm{off}}\boldsymbol{g}(\bar{z};z'), \end{aligned} \tag{33}$$

γ being the extended Keldysh contour of Fig. 2.c and $\boldsymbol{H}_{\mathrm{off}}$ is the off-diagonal part of $\boldsymbol{H}_s$. Using the relations (17) of Section 2.3 we find

$$\boldsymbol{\mathcal{G}}^{\mathrm{R,A}}_{C\alpha} = \boldsymbol{\mathcal{G}}^{\mathrm{R,A}}_{CC} \cdot \boldsymbol{H}_{C\alpha}\boldsymbol{g}^{\mathrm{R,A}}_{\alpha\alpha}, \quad \boldsymbol{\mathcal{G}}^{\mathrm{A}}_{\beta\alpha} = \delta_{\beta\alpha}\boldsymbol{g}^{\mathrm{A}}_{\beta\beta} + \boldsymbol{g}^{\mathrm{A}}_{\beta\beta}\boldsymbol{H}_{\beta C} \cdot \boldsymbol{\mathcal{G}}^{\mathrm{A}}_{CC} \cdot \boldsymbol{H}_{C\alpha}\boldsymbol{g}^{\mathrm{A}}_{\alpha\alpha}. \tag{34}$$

In Eq. (30) all matrix elements of $\boldsymbol{\mathcal{G}}^<$ are evaluated at times $(0;0)$. From Eq. (15) we see that $c^<(0;0) = \left[a^\rceil \star b^\lceil\right](0;0)$, due to the theta-functions in the retarded and advanced components. Therefore

$$\boldsymbol{\mathcal{G}}^<_{\beta C}(0;0) = \left[\boldsymbol{g}^\rceil_{\beta\beta}\boldsymbol{H}_{\beta C} \star \boldsymbol{\mathcal{G}}^\lfloor_{CC}\right](0;0), \quad \boldsymbol{\mathcal{G}}^<_{C\gamma}(0;0) = \left[\boldsymbol{\mathcal{G}}^\rceil_{CC} \star \boldsymbol{H}_{C\gamma}\boldsymbol{g}^\lfloor_{\gamma\gamma}\right](0;0), \tag{35}$$

and exploiting the first two relations in Eq. (19) we also find that

$$\boldsymbol{\mathcal{G}}^<_{\beta\gamma}(0;0) = \delta_{\beta\gamma}\boldsymbol{g}^<_{\beta\beta}(0;0) + \left[\boldsymbol{g}^\rceil_{\beta\beta}\boldsymbol{H}_{\beta C} \star \boldsymbol{\mathcal{G}}^{\mathrm{M}}_{CC} \star \boldsymbol{H}_{C\gamma}\boldsymbol{g}^\lfloor_{\gamma\gamma}\right](0;0). \tag{36}$$

Substituting Eqs. (34-35-36) into Eq. (30) and using the identities (24-25) for the Green function $\boldsymbol{g}$, we obtain the following expression for $\boldsymbol{Q}_\alpha(t)$

$$
\begin{aligned}
\boldsymbol{Q}_\alpha(t) = & \sum_{\beta=L,R} \left[\boldsymbol{G}^{\rm R}\cdot\boldsymbol{\Sigma}^<_\beta\cdot\left(\delta_{\beta\alpha}+\boldsymbol{G}^{\rm A}\cdot\boldsymbol{\Sigma}^{\rm A}_\alpha\right)\right](t;t) \\
& + \sum_{\beta=L,R} \left[\boldsymbol{G}^{\rm R}\cdot\boldsymbol{\Sigma}^\rceil\star\boldsymbol{G}^{\rm M}\star\boldsymbol{\Sigma}^\lceil_\beta\cdot\left(\delta_{\beta\alpha}+\boldsymbol{G}^{\rm A}\cdot\boldsymbol{\Sigma}^{\rm A}_\alpha\right)\right](t;t) \\
& + i\sum_{\beta=L,R} \boldsymbol{G}^{\rm R}(t;0)\left[\boldsymbol{G}^\rceil\star\boldsymbol{\Sigma}^\lceil_\beta\cdot\left(\delta_{\beta\alpha}+\boldsymbol{G}^{\rm A}\cdot\boldsymbol{\Sigma}^{\rm A}_\alpha\right)\right](0;t) \\
& + \left(\boldsymbol{G}^{\rm R}(t;0)\boldsymbol{G}^<(0;0) - i\left[\boldsymbol{G}^{\rm R}\cdot\boldsymbol{\Sigma}^\rceil\star\boldsymbol{G}^\lceil\right](t;0)\right)\left[\boldsymbol{G}^{\rm A}\cdot\boldsymbol{\Sigma}^{\rm A}_\alpha\right](0;t), \quad (37)
\end{aligned}
$$

where we have used the short-hand notation $\boldsymbol{G}\equiv\boldsymbol{\mathcal{G}}_{CC}$ and

$$
\boldsymbol{\Sigma}(z;z') = \sum_{\alpha=L,R}\boldsymbol{\Sigma}_\alpha, \quad \boldsymbol{\Sigma}_\alpha(z;z') = \boldsymbol{H}_{C\alpha}\,\boldsymbol{g}_{\alpha\alpha}(z;z')\boldsymbol{H}_{\alpha C} \tag{38}
$$

is the so-called embedding self-energy which accounts for hopping in and out of region C.

Having the quantity $\boldsymbol{Q}_\alpha(t)$ we can calculate the exact total current $I_\alpha(t)$ of an interacting system of electrons. Eq. (29) allows for studying transient effects and more generally any kind of time-dependent current responses. In the long time limit

$$
\lim_{t\to\infty}\boldsymbol{Q}_\alpha(t) = \left[\boldsymbol{G}^{\rm R}\cdot\boldsymbol{\Sigma}^<_\alpha + \boldsymbol{G}^{\rm R}\cdot\boldsymbol{\Sigma}^<\cdot\boldsymbol{G}^{\rm A}\cdot\boldsymbol{\Sigma}^{\rm A}_\alpha\right](t;t) \tag{39}
$$

provided $\boldsymbol{G}$ and $\boldsymbol{\Sigma}$ tend to zero when the separation between their time arguments increases (in this case, it is only the first term on the r.h.s. of Eq. (37) that does not vanish). This condition is not stringent and is fulfilled provided the electrode states form a continuum and the local density of states in the central region C is a smooth function. In the next Section we investigate under what circumstances a steady current I_α develops in the long-time limit. We will also discuss the dependence of I_α on the history of the external potential.

3.3 Steady state and history dependence

In this Section we show that a steady state develops provided 1) the KS Hamiltonian $\boldsymbol{H}_s(t)$ *globally* converges to an asymptotic KS Hamiltonian $\boldsymbol{H}^\infty_s$ when $t\to\infty$ and 2) the electrodes form a continuum of states (thermodynamic limit) and the local density of states is a smooth function in the central region.

Let us define the asymptotic KS Hamiltonian of electrode α as $\boldsymbol{H}^\infty_{\alpha\alpha} = \lim_{t\to\infty}\boldsymbol{H}_{\alpha\alpha}(t)$. The retarded/advanced component of the uncontacted Green function $\boldsymbol{g}$ behaves like

$$
\lim_{t\to\infty}\boldsymbol{g}^{\rm R}_{\alpha\alpha}(t,0) = i\,{\rm e}^{-i\boldsymbol{H}^\infty_{\alpha\alpha}t}\boldsymbol{\mathcal{S}}, \qquad \lim_{t\to\infty}\boldsymbol{g}^{\rm A}_{\alpha\alpha}(0,t) = -i\,\boldsymbol{\mathcal{S}}^\dagger{\rm e}^{i\boldsymbol{H}^\infty_{\alpha\alpha}t} \tag{40}
$$

where $\boldsymbol{\mathcal{S}}$ is a unitary operator and it is defined according to

$$\boldsymbol{\mathcal{S}} = \lim_{t\to\infty} \frac{T\left\{\mathrm{e}^{-i\int_0^t \boldsymbol{H}_{\alpha\alpha}(t')dt'}\right\}}{\mathrm{e}^{-i\boldsymbol{H}^{\infty}_{\alpha\alpha}t}}, \tag{41}$$

T being the time-ordering operator. In terms of diagonalising one-body states $|\psi^{\infty}_{m\alpha}\rangle$ of $\boldsymbol{H}^{\infty}_{\alpha\alpha}$ with eigenvalues $\varepsilon^{\infty}_{m\alpha}$, the lesser component of the embedding self-energy, defined in Eq. (38), can be written as

$$\begin{aligned}\lim_{t,t'\to\infty} \boldsymbol{\Sigma}^{<}_{\alpha}(t;t') &= \lim_{t,t'\to\infty} \boldsymbol{H}_{C\alpha}\, \boldsymbol{g}^{\mathrm{R}}_{\alpha\alpha}(t;0)\boldsymbol{g}^{<}_{\alpha\alpha}(0;0)\boldsymbol{g}^{\mathrm{A}}_{\alpha\alpha}(0;t')\boldsymbol{H}_{\alpha C} \\ &= i\sum_{m,m'} \mathrm{e}^{-i[\varepsilon^{\infty}_{m\alpha}t-\varepsilon^{\infty}_{m'\alpha}t']} \\ &\times \boldsymbol{H}_{C\alpha}|\psi^{\infty}_{m\alpha}\rangle\langle\psi^{\infty}_{m\alpha}|f(\boldsymbol{\mathcal{S}}\boldsymbol{H}_{\alpha\alpha}(0)\boldsymbol{\mathcal{S}}^{\dagger})|\psi^{\infty}_{m'\alpha}\rangle\langle\psi^{\infty}_{m'\alpha}|\boldsymbol{H}_{\alpha C}, \end{aligned} \tag{42}$$

where we have taken into account that $\boldsymbol{g}^{<}_{\alpha\alpha}(0;0) = if(\boldsymbol{H}_{\alpha\alpha}(0))$. The left and right contraction with a nonsingular hopping matrix $\boldsymbol{H}_{\alpha C}$ causes a perfect destructive interference for states with $|\varepsilon^{\infty}_{m\alpha} - \varepsilon^{\infty}_{m'\alpha}| \gtrsim 1/(t+t')$ and hence the restoration of translational invariance in time

$$\lim_{t,t'\to\infty} \boldsymbol{\Sigma}^{<}_{\alpha}(t;t') = i\sum_{m} f_{m\alpha}\boldsymbol{\Gamma}_{m\alpha}\mathrm{e}^{-i\varepsilon^{\infty}_{m\alpha}(t-t')}, \tag{43}$$

where $f_{m\alpha} = \langle\psi^{\infty}_{m\alpha}|f(\boldsymbol{\mathcal{S}}\boldsymbol{H}_{\alpha\alpha}(0)\boldsymbol{\mathcal{S}}^{\dagger})|\psi^{\infty}_{m\alpha}\rangle$ while $\boldsymbol{\Gamma}_{m\alpha} = \boldsymbol{H}_{C\alpha}|\psi^{\infty}_{m\alpha}\rangle\langle\psi^{\infty}_{m\alpha}|\boldsymbol{H}_{\alpha C}$. In principle, there may be degeneracies which require a diagonalisation to be performed for states on the energy shell. The above *dephasing mechanism* is the key ingredient for a steady state to develop. Substituting Eq. (43) into Eq. (39) we obtain for the steady state current

$$\begin{aligned} I^{(\mathrm{S})}_{\alpha} =& -2e\sum_{m\beta} f_{m\beta}\mathrm{Tr}_C\left\{\boldsymbol{G}^{\mathrm{R}}(\varepsilon^{\infty}_{m\beta})\boldsymbol{\Gamma}_{m\beta}\boldsymbol{G}^{\mathrm{A}}(\varepsilon^{\infty}_{m\beta})\mathrm{Im}[\boldsymbol{\Sigma}^{\mathrm{A}}_{\alpha}(\varepsilon^{\infty}_{m\beta})]\right\} \\ & -2e\sum_{m} f_{m\alpha}\mathrm{Tr}_C\left\{\boldsymbol{\Gamma}_{m\alpha}\mathrm{Im}[\boldsymbol{G}^{\mathrm{R}}(\varepsilon^{\infty}_{m\alpha})]\right\} \end{aligned} \tag{44}$$

with

$$\boldsymbol{G}^{\mathrm{R,A}}(\varepsilon) = \frac{1}{\varepsilon\boldsymbol{1}_C - \boldsymbol{H}^{\infty}_{CC} - \boldsymbol{\Sigma}^{\mathrm{R,A}}(\varepsilon)}. \tag{45}$$

The imaginary part of $\boldsymbol{G}^{\mathrm{R}}$ is simply given by $\boldsymbol{G}^{\mathrm{R}}\mathrm{Im}[\boldsymbol{\Sigma}^{\mathrm{R}}]\boldsymbol{G}^{\mathrm{A}}$. By definition we have

$$\boldsymbol{\Sigma}^{\mathrm{R,A}}_{\alpha}(\varepsilon) = \boldsymbol{H}_{C\alpha}\frac{1}{\varepsilon\boldsymbol{1}_{\alpha} - \boldsymbol{H}^{\infty}_{\alpha\alpha} \pm i\eta}\boldsymbol{H}_{\alpha C} \tag{46}$$

and hence

$$\mathrm{Im}\left[\boldsymbol{\Sigma}^{\mathrm{R,A}}_{\alpha}(\varepsilon)\right] = \mp\pi\sum_{m}\delta(\varepsilon - \varepsilon^{\infty}_{m\alpha})\boldsymbol{\Gamma}_{m\alpha}. \tag{47}$$

Using the above identity, the steady-state current can be rewritten in a Landauer-like [22] form

$$I_R^{(\mathrm{S})} = -e\sum_m [f_{mL}\mathcal{T}_{mL} - f_{mR}\mathcal{T}_{mR}] = -I_L^{(\mathrm{S})}. \tag{48}$$

In the above formula $\mathcal{T}_{mR} = \sum_n \mathcal{T}_{mR}^{nL}$ and $\mathcal{T}_{mL} = \sum_n \mathcal{T}_{mL}^{nR}$ are the TDDFT transmission coefficients expressed in terms of the quantities

$$\mathcal{T}_{m\alpha}^{n\beta} = 2\pi\delta(\varepsilon_{m\alpha}^{\infty} - \varepsilon_{n\beta}^{\infty})\mathrm{Tr}_C\left\{\boldsymbol{G}^{\mathrm{R}}(\varepsilon_{m\alpha}^{\infty})\boldsymbol{\Gamma}_{m\alpha}\boldsymbol{G}^{\mathrm{A}}(\varepsilon_{n\beta}^{\infty})\boldsymbol{\Gamma}_{n\beta}\right\} = \mathcal{T}_{n\beta}^{m\alpha}. \tag{49}$$

Despite the formal analogy with the Landauer formula, Eq. (48) contains an important conceptual difference since $f_{m\alpha}$ is not simply given by the Fermi distribution function. For example, if the induced change in effective potential varies widely in space deep inside the electrodes, the band structure of the α-electrode Hamiltonian $\boldsymbol{\mathcal{S}}\boldsymbol{H}_{\alpha\alpha}(0)\boldsymbol{\mathcal{S}}^{\dagger}$ might differ from that of $\boldsymbol{H}_{\alpha\alpha}^{\infty}$. However, for metallic electrodes with a macroscopic cross section the switching on of an electric field excites plasmon oscillations which dynamically screen the external disturbance. Such a metallic screening prevents any rearrangements of the initial equilibrium bulk-density, provided the time-dependent perturbation is slowly varying during a typical plasmon time-scale (which is usually less than a fs). Thus, the KS potential v_s undergoes a uniform time-dependent shift deep inside the left and right electrodes and the KS potential-drop is entirely limited to the central region. Denoting with $\Delta v_\alpha(t)$ the difference in electrode α between the KS potential at time t and the KS potential at negative times, $\Delta v_\alpha(t) = v_s(\mathbf{r}\in\alpha, t) - v_s(\mathbf{r}\in\alpha, 0)$, to leading order in $1/N$ we then have

$$\boldsymbol{H}_{\alpha\alpha}(t) = \boldsymbol{H}_{\alpha\alpha}(0) + \mathbf{1}_\alpha \Delta v_\alpha(t), \tag{50}$$

meaning that $\boldsymbol{H}_{\alpha\alpha}^{\infty} = \boldsymbol{H}_{\alpha\alpha}(0) + \mathbf{1}_\alpha \Delta v_\alpha^{\infty}$. Hence, except for corrections which are of lower order with respect to the system size, $\boldsymbol{\mathcal{S}}\boldsymbol{H}_{\alpha\alpha}(0)\boldsymbol{\mathcal{S}}^{\dagger} = \boldsymbol{H}_{\alpha\alpha}(0)$ and

$$f_{m\alpha} = f(\varepsilon_{m\alpha}^{\infty} - \Delta v_\alpha^{\infty}). \tag{51}$$

The formula for the current can be further manipulated when Eq. (51) holds. Let us write the embedding self-energy as the sum of a real and imaginary part $\boldsymbol{\Sigma}_\alpha^{\mathrm{R,A}}(\varepsilon) = \boldsymbol{\Lambda}_\alpha(\varepsilon) \mp i\boldsymbol{\Gamma}_\alpha(\varepsilon)/2$. Using Eq. (47) we can rewrite the transmission coefficients as

$$\mathcal{T}_{mR} = \mathrm{Tr}_C\left\{\boldsymbol{G}^{\mathrm{R}}(\varepsilon_{mR}^{\infty})\boldsymbol{\Gamma}_{mR}\boldsymbol{G}^{\mathrm{A}}(\varepsilon_{mR}^{\infty})\boldsymbol{\Gamma}_L(\varepsilon_{mR}^{\infty})\right\}, \tag{52}$$

$$\mathcal{T}_{mL} = \mathrm{Tr}_C\left\{\boldsymbol{G}^{\mathrm{R}}(\varepsilon_{mL}^{\infty})\boldsymbol{\Gamma}_{mL}\boldsymbol{G}^{\mathrm{A}}(\varepsilon_{mL}^{\infty})\boldsymbol{\Gamma}_R(\varepsilon_{mL}^{\infty})\right\}. \tag{53}$$

Substituting these expressions in Eq. (48) and taking into account Eq. (51)

we obtain

$$I_R^{(\mathrm{S})} = -e \int \frac{d\varepsilon}{2\pi} \left[f(\varepsilon - \Delta v_L^\infty) - f(\varepsilon - \Delta v_R^\infty) \right] \mathrm{Tr}_C \left\{ \boldsymbol{G}^{\mathrm{R}}(\varepsilon) \boldsymbol{\Gamma}_L(\varepsilon) \boldsymbol{G}^{\mathrm{A}}(\varepsilon) \boldsymbol{\Gamma}_R(\varepsilon) \right\}. \tag{54}$$

In the above equation the Green functions are calculated from Eq. (45). The Hamiltonian $\boldsymbol{H}_{CC}^\infty$ is the KS Hamiltonian $\boldsymbol{H}_s(t \to \infty)$ projected on region C and can be obtained by evolving the system for very long times. According to the Runge-Gross theorem, $\boldsymbol{H}_{CC}^\infty$ depends on how the system was prepared at $t = 0$ (in our case the system is contacted and in thermal equilibrium) and on the full history of the time-dependent density. Therefore, *the use of Eq. (54) in the context of static DFT is generally not correct*. Indeed, static DFT is an equilibrium theory while here we are dealing with a non-equilibrium process. One might argue that in the linear-response regime the static DFT approach is free from the above criticism. Unfortunately, this is not the case. Denoting with δv_α^∞ the small change Δv_α^∞ of the effective potential in electrode α and with $\delta I_R^{(\mathrm{S})}$ the corresponding current response, to first order in δv_α^∞ Eq. (54) yields

$$\delta I_R^{(\mathrm{S})} = -e \int \frac{d\varepsilon}{2\pi} \frac{\partial f(\varepsilon)}{\partial \varepsilon} \mathrm{Tr}_C \left\{ \boldsymbol{G}_0^{\mathrm{R}}(\varepsilon) \boldsymbol{\Gamma}_{0,L}(\varepsilon) \boldsymbol{G}_0^{\mathrm{A}}(\varepsilon) \boldsymbol{\Gamma}_{0,R}(\varepsilon) \right\} (\delta v_R^\infty - \delta v_L^\infty). \tag{55}$$

The Green functions and the $\boldsymbol{\Gamma}$'s in Eq. (55) refer to the system in equilibrium and static DFT approaches can be used to evaluate the trace. However, DFT is not enough to calculate the change δv_α^∞. Indeed

$$\delta v_\alpha^\infty = \lim_{t\to\infty} \lim_{x\to\pm\infty} \left[\delta v_{\mathrm{ext}}(\boldsymbol{r}, t) + \delta V_{\mathrm{H}}(\boldsymbol{r}, t) + \delta v_{\mathrm{xc}}(\boldsymbol{r}, t) \right], \tag{56}$$

where x is the longitudinal coordinate, the plus sign applies for $\alpha = R$ and the minus sign for $\alpha = L$. In the above equation v_{ext} is the external potential and V_{H} is the Hartree potential; their sum gives the electrostatic Coulomb potential v_{C},

$$\delta v_{\alpha,\mathrm{C}} = \lim_{t\to\infty} \lim_{x\to\pm\infty} \left[\delta v_{\mathrm{ext}}(\boldsymbol{r}, t) + \delta V_{\mathrm{H}}(\boldsymbol{r}, t) \right]. \tag{57}$$

The variation δv_{xc} of the exchange-correlation potential can be expressed in terms of the exchange-correlation kernel $f_{\mathrm{xc}}(\boldsymbol{r}, t; \boldsymbol{r}', t') = \delta v_{\mathrm{xc}}(\boldsymbol{r}, t)/\delta n(\boldsymbol{r}', t')$

$$\delta v_{\alpha,\mathrm{xc}} = \lim_{t\to\infty} \lim_{x\to\pm\infty} \delta v_{\mathrm{xc}}(\boldsymbol{r}, t) = \lim_{t\to\infty} \lim_{x\to\pm\infty} \int \mathrm{d}\boldsymbol{r}' \int \mathrm{d}t' f_{\mathrm{xc}}(\boldsymbol{r}, t; \boldsymbol{r}', t') \delta n(\boldsymbol{r}', t'). \tag{58}$$

The kernel f_{xc} depends only on the difference $t - t'$. We denote by $f_{\alpha,\mathrm{xc}}(\boldsymbol{r}', \omega)$ the Fourier transform of f_{xc} evaluated at $x = \pm\infty$ for $\alpha = R, L$. Then

$$\delta v_{\alpha,\mathrm{xc}} = \lim_{t\to\infty} \int \frac{d\omega}{2\pi} \mathrm{e}^{-i\omega t} \int \mathrm{d}\boldsymbol{r}' f_{\alpha,\mathrm{xc}}(\boldsymbol{r}', \omega) \delta n(\boldsymbol{r}', \omega) \tag{59}$$

with $\delta n(\boldsymbol{r}, \omega)$ the Fourier transform of $\delta n(\boldsymbol{r}, t)$. Rewriting δv_α^∞ as $\delta v_{\alpha,\mathrm{C}} + \delta v_{\alpha,\mathrm{xc}}$

and taking into account Eq. (59), the current response $\delta I_R^{(\mathrm{S})}$ in Eq. (55) can also be written as

$$\delta I_R^{(\mathrm{S})} = -e \int \frac{d\varepsilon}{2\pi} \frac{\partial f(\varepsilon)}{\partial \varepsilon} T(\varepsilon) \left[(\delta v_{R,\mathrm{C}} - \delta v_{L,\mathrm{C}}) + \lim_{t\to\infty} \int \frac{d\omega}{2\pi} \mathrm{e}^{-i\omega t} \right. \\ \left. \times \int \mathrm{d}\boldsymbol{r}' \left(f_{R,\mathrm{xc}}(\boldsymbol{r}', \omega) - f_{L,\mathrm{xc}}(\boldsymbol{r}', \omega) \right) \delta n(\boldsymbol{r}', \omega) \right] \tag{60}$$

with $T(\varepsilon) = \mathrm{Tr}_C \left\{ \boldsymbol{G}_0^{\mathrm{R}}(\varepsilon) \boldsymbol{\Gamma}_{0,L}(\varepsilon) \boldsymbol{G}_0^{\mathrm{A}}(\varepsilon) \boldsymbol{\Gamma}_{0,R}(\varepsilon) \right\}$. At zero temperature $\partial f(\varepsilon)/\partial\varepsilon = \delta(\varepsilon - \varepsilon_F)$, with ε_F the Fermi energy, and Eq. (60) becomes

$$\delta I_R^{(\mathrm{S})} = G_{\mathrm{KS}}(\varepsilon_F) \left[(\delta v_{R,\mathrm{C}} - \delta v_{L,\mathrm{C}}) + \lim_{t\to\infty} \int \frac{d\omega}{2\pi} \mathrm{e}^{-i\omega t} \right. \\ \left. \times \int \mathrm{d}\boldsymbol{r}' \left(f_{R,\mathrm{xc}}(\boldsymbol{r}', \omega) - f_{L,\mathrm{xc}}(\boldsymbol{r}', \omega) \right) \delta n(\boldsymbol{r}', \omega) \right] \tag{61}$$

where $G_{\mathrm{KS}}(\varepsilon_F) = -eT(\varepsilon_F)/2\pi$ is the conductance of the KS system. We conclude that *also in the linear-response regime static DFT is not appropriate* for calculating the conductance since dynamical exchange-correlation effects might contribute through the last term in Eq. (61). Eq. (61) can also be obtained within the framework of time-dependent current density functional theory as it has been shown in Ref. [23].

We emphasize that the steady-state current in Eq. (48) results from a pure dephasing mechanism in the fictitious noninteracting problem. The damping effects of scattering are described by A_{xc} and v_{xc}. Furthermore, the current depends only on the asymptotic value of the KS potential, $v_s(\mathbf{r}, t \to \infty)$. However, $v_s(\mathbf{r}, t \to \infty)$ might depend on the history of the external applied potential and the resulting steady-state current might be history dependent. In these cases the full time evolution can not be avoided. In the case of Time Dependent Local Density Approximation (TDLDA), the exchange-correlation potential v_{xc} depends only locally on the instantaneous density and has no memory at all. If the density tends to a constant, so does the KS potential v_s, which again implies that the density tends to a constant. Owing to the non-linearity of the problem there might still be more than one steady-state solution or none at all. We are currently investigating the possibility of having more than one steady state solution.

4 Quantum transport: A practical scheme based on TDDFT

The theory presented in the previous Sections allows us to calculate the time-dependent current in terms of the Green function $\boldsymbol{\mathcal{G}}_{CC} = \boldsymbol{G}$ projected in the central region. In practise, it is computationally very expensive to propagate $\boldsymbol{G}(z; z')$ in time (because it depends on two time variables) and also calculate $\boldsymbol{Q}_\alpha$ from Eq. (37). Here we describe a feasible numerical scheme based on the propagation of KS orbitals. We remind the reader that our electrode-junction-electrode system is infinite and non-periodic. Since one can in practice only deal with finite systems we will propagate KS orbitals projected in the central region C by applying the correct boundary conditions.[10]

We specialize the discussion to nonmagnetic systems at zero temperature and we denote with $\psi_s(\boldsymbol{r}, 0) \equiv \langle \boldsymbol{r}|\psi_s(0)\rangle$ the eigenstates of $\boldsymbol{H}_s(t < 0)$. The time dependent density can be computed in the usual way by $n(\boldsymbol{r}, t) = \sum_{\text{occ}} |\psi_s(\boldsymbol{r}, t)|^2$, where the sum is over the occupied Kohn-Sham orbitals and $|\psi_s(t)\rangle$ is the solution of the KS equation of TDDFT $i\frac{\mathrm{d}}{\mathrm{d}t}|\psi_s(t)\rangle = \boldsymbol{H}_s(t)|\psi_s(t)\rangle$. Using the continuity equation, we can write the total current $I_\alpha(t)$ of Eq. (26) as

$$\begin{aligned} I_\alpha(t) &= -e \sum_{\text{occ}} \int_\alpha \mathrm{d}\boldsymbol{r} \boldsymbol{\nabla} \cdot \mathrm{Im}\left[\psi_s^*(\boldsymbol{r}, t)\boldsymbol{\nabla}\psi_s(\boldsymbol{r}, t)\right] \\ &= -e \sum_{\text{occ}} \int_{S_\alpha} \mathrm{d}\sigma\, \hat{\mathbf{n}} \cdot \mathrm{Im}\left[\psi_s^*(\boldsymbol{r}, t)\boldsymbol{\nabla}\psi_s(\boldsymbol{r}, t)\right] \end{aligned} \tag{62}$$

where $\hat{\mathbf{n}}$ is the unit vector perpendicular to the surface element $\mathrm{d}\sigma$ and the surface S_α is perpendicular to the longitudinal geometry of our system. From Eq. (62) we conclude that in order to calculate $I_\alpha(t)$ we only need to know the time-evolved KS orbitals in region C. This is possible provided we know the dynamics of the remote parts of the system. As at the end of Section 3.3, we restrict ourselves to metallic electrodes. Then, the external potential and the disturbance introduced by the device region are screened deep inside the electrodes. As the system size increases, the remote parts are less disturbed by the junction and the density inside the electrodes approaches the equilibrium bulk-density. Thus, the macroscopic size of the electrodes leads to an enormous simplification since the initial-state self-consistency is not disturbed far away from the constriction. Partitioning the KS Hamiltonian as in Eq. (27), the time-dependent Schrödinger equation reads

$$i\frac{\mathrm{d}}{\mathrm{d}t}\begin{bmatrix} |\psi_L\rangle \\ |\psi_C\rangle \\ |\psi_R\rangle \end{bmatrix} = \begin{bmatrix} \boldsymbol{H}_{LL} & \boldsymbol{H}_{LC} & 0 \\ \boldsymbol{H}_{CL} & \boldsymbol{H}_{CC} & \boldsymbol{H}_{CR} \\ 0 & \boldsymbol{H}_{RC} & \boldsymbol{H}_{RR} \end{bmatrix} \begin{bmatrix} |\psi_L\rangle \\ |\psi_C\rangle \\ |\psi_R\rangle \end{bmatrix}, \tag{63}$$

where $|\psi_\alpha\rangle$ is the projected wave-function onto the region $\alpha = L, R, C$. We can

solve the differential equation for ψ_L and ψ_R in terms of the retarded Green function $\boldsymbol{g}^{\mathrm{R}}_{\alpha\alpha}$. Then, we have for $\alpha = L, R$

$$|\psi_\alpha(t)\rangle = i\boldsymbol{g}^{\mathrm{R}}_{\alpha\alpha}(t,0)|\psi_\alpha(0)\rangle + \int_0^t \mathrm{d}t' \boldsymbol{g}^{\mathrm{R}}_{\alpha\alpha}(t,t')\boldsymbol{H}_{\alpha C}|\psi_C(t')\rangle. \tag{64}$$

Using Eq. (64), the equation for ψ_C can be written as

$$\begin{aligned} i\frac{\mathrm{d}}{\mathrm{d}t}|\psi_C(t)\rangle = &\boldsymbol{H}_{CC}(t)|\psi_C(t)\rangle + \int_0^t \mathrm{d}t' \boldsymbol{\Sigma}^{\mathrm{R}}(t,t')|\psi_C(t')\rangle \\ &+ i\sum_{\alpha=L,R} \boldsymbol{H}_{C\alpha}\boldsymbol{g}^{\mathrm{R}}_{\alpha\alpha}(t,0)|\psi_\alpha(0)\rangle, \end{aligned} \tag{65}$$

where $\boldsymbol{\Sigma}^{\mathrm{R}} = \sum_{\alpha=L,R} \boldsymbol{H}_{C\alpha}\boldsymbol{g}^{\mathrm{R}}_{\alpha\alpha}\boldsymbol{H}_{\alpha C}$, in accordance with Eq. (38). Thus, for any given KS orbital we can evolve its projection onto the central region by solving Eq. (65) in region C. Eq. (65) has also been derived elsewhere (for static Hamiltonians).[24] To summarize, all the complexity of the infinite electrode-junction-electrode system has been reduced to the solution of an open quantum-mechanical system (the central region C) with proper time-dependent boundary conditions.

Equation (65) is the central equation of our numerical approach to time-dependent transport. It is a reformulation of the original time-dependent Schrödinger equation (63) of the full system in terms of an equation for the central (device) region only. The coupling to the leads is taken into account by the lead Green functions $\boldsymbol{g}^{\mathrm{R}}_{\alpha\alpha}, \alpha = L, R$. Eq. (65) has the structure of a time-dependent Schrödinger equation with two extra terms. The first term describes the injection of particles induced by a non-vanishing projection of the initial wave-function onto the leads. The second term involves the self-energy $\boldsymbol{\Sigma}^{\mathrm{R}}$ and the wavefunction in the central region at previous times during the propagation. We will denote it as the memory integral. We should remark here that these memory effects are of different origin than those which are usually discussed in the context of TDDFT[25,26]. The latter ones arise from the dependence of the exchange-correlation functional on the full history of the time-dependent density. Most density-based functionals used at present rely on the adiabatic approximation therefore ignoring the functional dependence on past time-dependent densities (Ref. [27]).

Equation (65) is first order in time, therefore we need to specify an initial state which is to be propagated. We want to study the time evolution of systems perturbed out of their equilibrium ground state. Of course, the ground state of our noninteracting system is the Slater determinant of the occupied eigenstates of the full, extended Hamiltonian in equilibrium, $\boldsymbol{H}_s(t < 0)$. The practical question then arises how one can obtain these eigenstates and how one can propagate them in time without having to deal explicitly with the extended Hamiltonian. Below we show how we have coped with these problems.

Let us consider our electrode-junction-electrode system in equilibrium ($t < 0$) and let $\psi_s(\boldsymbol{r}) = \psi_{Ej}(\boldsymbol{r})$ be the j-th degenerate eigenstate of energy E of the KS Hamiltonian $\boldsymbol{H}_s$. The Green functions $\boldsymbol{\mathcal{G}}^{\mathrm{R,A}}(t;t')$ and $\boldsymbol{\mathcal{G}}^{<}(t;t')$ of the undisturbed system depend only on the difference $t-t'$. In absence of magnetic fields $\boldsymbol{H}_s$ is invariant under time-reversal and the imaginary part of the Fourier transformed $\boldsymbol{\mathcal{G}}^{\mathrm{R}}$ is simply given by

$$-\frac{1}{\pi}\mathrm{Im}\,[\langle \boldsymbol{r}|\boldsymbol{\mathcal{G}}(E)|\boldsymbol{r}'\rangle] = \sum_{E'}\delta(E-E')\sum_{j=1}^{d_{E'}}\psi_{E'j}(\boldsymbol{r})\psi^*_{E'j}(\boldsymbol{r}')\,. \tag{66}$$

Multiplying Eq. (66) by $\psi^*_{Em}(\boldsymbol{r})\psi_{En}(\boldsymbol{r}')$ and integrating over $\boldsymbol{r}$ and $\boldsymbol{r}'$ in region C we obtain

$$\begin{aligned}-\frac{1}{\pi}\int_C \mathrm{d}\boldsymbol{r}\int_C \mathrm{d}\boldsymbol{r}'\psi^*_{Em}(\boldsymbol{r})\mathrm{Im}\,[\langle \boldsymbol{r}|\boldsymbol{\mathcal{G}}(E)|\boldsymbol{r}'\rangle]\,\psi_{En}(\boldsymbol{r}') \\ = \sum_{E'}\delta(E-E')\sum_{j=1}^{d_{E'}}S_{mj}(E')S_{jn}(E'),\end{aligned} \tag{67}$$

where

$$S_{mj}(E) \equiv \int_C \mathrm{d}\boldsymbol{r}\;\psi^*_{Em}(\boldsymbol{r})\psi_{Ej}(\boldsymbol{r}) = S^*_{jm}(E) \tag{68}$$

is the overlap matrix in region C between degenerate states. This matrix is Hermitian and can be diagonalized, i.e.,

$$\sum_{j=1}^{d_E} S_{mj}(E)a^{(l)}_j(E) = \lambda_l(E)a^{(l)}_m(E). \tag{69}$$

Next, we multiply Eq. (67) by $a^{(l)^*}_m(E)a^{(l')}_n(E)$ and sum over m and n. The result can be written in terms of the new eigenfunctions $a_{El}(\boldsymbol{r}) = \sum_{n=1}^{d_E} a^{(l)}_n(E)\psi_{En}(\boldsymbol{r})$ as

$$-\frac{1}{\pi}\int_C \mathrm{d}\boldsymbol{r}\int_C \mathrm{d}\boldsymbol{r}'a^*_{El}(\boldsymbol{r})\mathrm{Im}\,[\langle \boldsymbol{r}|\boldsymbol{\mathcal{G}}(E)|\boldsymbol{r}'\rangle]\,a_{El'}(\boldsymbol{r}') = \delta_{ll'}\lambda^2_l(E)\sum_{E'}\delta(E-E'), \tag{70}$$

where we have used Eq. (69) and the orthonormality of the S-matrix eigenvectors: $\sum_{j=1}^{d_E} a^{(l)^*}_j(E)a^{(l')}_j(E) = \delta_{ll'}$. Equation (70) shows explicitly that the functions $a_{Ej}(\boldsymbol{r})$ diagonalize $\mathrm{Im}\,[\boldsymbol{\mathcal{G}}_{CC}(E)]$ in the central region and that the eigenvalues are positive. Since any linear combination of degenerate eigenstates is again an eigenstate, diagonalizing $\mathrm{Im}\,[\boldsymbol{\mathcal{G}}_{CC}(E)]$ gives us one set of linearly independent, degenerate eigenstates of energy E. In our practical im-

plementation described in more detail in Section 5, we diagonalize

$$-\frac{1}{\pi D_C(E)}\mathrm{Im}\left[\boldsymbol{\mathcal{G}}_{CC}(E)\right] \tag{71}$$

where $D_C(E) = -\frac{1}{\pi}\mathrm{Tr}\left\{\mathrm{Im}\left[\boldsymbol{\mathcal{G}}_{CC}(E)\right]\right\}$ is the total density of states in the central region. If we use N_g grid points to describe the central region, the diagonalization in principle gives N_g eigenvectors but only a few have the physical meaning of extended eigenstates at this energy. It is, however, very easy to identify the physical states by looking at the eigenvalues: at a given energy E only d_E eigenvalues are nonvanishing and they always add up to unity. The corresponding states are the physical ones. All the other eigenvalues are zero (or numerically close to zero) and the corresponding states have no physical meaning.

The procedure described above gives the correct extended eigenstates only up to a normalization factor. When diagonalizing Eq. (71) with typical library routines one obtains eigenvectors which are normalized to the central region. Physically this might be incorrect. It is possible to fix the normalization by matching the wavefunction for the central region to the known form (and normalization) of the wavefunction in the macroscopic leads.

It should be emphasized that the procedure described here for the extraction of eigenstates of the extended system from $\boldsymbol{\mathcal{G}}_{CC}(E)$ only works in practice if E is in the continuous part of the spectrum due to the sharp peak of the delta function in the discrete part of the spectrum. Eigenstates in the discrete part of the spectrum can be found by considering the original Schrödinger equation for the full system: $\boldsymbol{H}_s\psi = E\psi$. Using again the block structure of the Hamiltonian this can be transformed into an effective Schrödinger equation for an *energy-dependent* Hamiltonian for the central region only:

$$\left(\boldsymbol{H}_{CC} + \sum_{\alpha=L,R} \boldsymbol{H}_{C\alpha}\frac{1}{E\mathbf{1}_\alpha - \boldsymbol{H}_{\alpha\alpha}}\boldsymbol{H}_{\alpha C}\right)|\psi_C\rangle = E|\psi_C\rangle. \tag{72}$$

This equation has solutions only for certain values of E which are the discrete eigenenergies of the full Hamiltonian $\boldsymbol{H}_s$. Since the left and right electrodes form a continuum, the dimension of the kernel of $(E - \boldsymbol{H}_{\alpha\alpha})$ is zero for those energies E in the discrete part of the spectrum. We also notice that the second term in parenthesis in Eq. (72) is nothing but the real part of the retarded/advanced self-energy in equilibrium, see Eq. (47). Bound states as well as fully reflected waves will contribute to the density but not to the current and might play a role in the description of charge-accumulation in molecular transport, as, e.g., in Coulomb blockade phenomena. In our TDDFT formulation bound states and fully reflected waves also play an extra role, since they are needed for calculating the effective potential v_s (which is a functional of the density) which is in turn used for extracting all extended states.

In order to calculate the longitudinal current in an electrode-junction-electrode system we need to propagate the Kohn-Sham orbitals. The main difficulty stems from the macroscopic size of the electrodes whose remote parts, ultimately, are taken infinitely far away from the central, explicitly treated, scattering region C.

The problem can be solved by imposing transparent boundary conditions[28] at the electrode-junction interfaces. Efficient algorithms have been proposed for wave-packets initially *localized* in the scattering region and for Hamiltonians constant in time. In this Section we describe an algorithm well suited for delocalized initial states, as well as for localized ones, evolving with a time-dependent Hamiltonian.

Let $\boldsymbol{H}_s(t)$ be the time-dependent KS Hamiltonian. We partition $\boldsymbol{H}_s(t)$ as in Section 3.2. The explicitly treated region C includes the first few atomic layers of the left and right electrodes. The boundaries of this region are chosen in such a way that the density outside C is accurately described by an equilibrium bulk density. It is convenient to write $\boldsymbol{H}_{\alpha\alpha}(t)$, with $\alpha = L, R$, as the sum of a term $\boldsymbol{H}^0_{\alpha\alpha} = \boldsymbol{H}_{\alpha\alpha}(0)$ which is constant in time and another term $\boldsymbol{U}_\alpha(t)$ which is explicitly time-dependent, $\boldsymbol{H}_{\alpha\alpha}(t) = \boldsymbol{H}^0_{\alpha\alpha} + \boldsymbol{U}_\alpha(t)$. In configuration space $\boldsymbol{U}_\alpha(t)$ is diagonal at any time t since the KS potential is local in space. Furthermore, the diagonal elements $U_\alpha(\boldsymbol{r}, t)$ are spatially constant for metallic electrodes. Thus, $\boldsymbol{U}_\alpha(t) = U_\alpha(t)\mathbf{1}_\alpha$ and $U_L(t) - U_R(t)$ is the total potential drop across the central region. We write $\boldsymbol{H}_s(t) = \tilde{\boldsymbol{H}}(t) + \boldsymbol{U}(t)$ with

$$\tilde{\boldsymbol{H}}(t) = \begin{bmatrix} \boldsymbol{H}^0_{LL} & \boldsymbol{H}_{LC} & 0 \\ \boldsymbol{H}_{CL} & \boldsymbol{H}_{CC}(t) & \boldsymbol{H}_{CR} \\ 0 & \boldsymbol{H}_{RC} & \boldsymbol{H}^0_{RR} \end{bmatrix}, \quad \text{and} \quad \boldsymbol{U}(t) = \begin{bmatrix} U_L(t)\mathbf{1}_L & 0 & 0 \\ 0 & 0 & 0 \\ 0 & 0 & U_R(t)\mathbf{1}_R \end{bmatrix}. \tag{73}$$

In this way, the only term in $\tilde{\boldsymbol{H}}(t)$ that depends on t is $\boldsymbol{H}_{CC}(t)$. For any given initial state $|\psi(0)\rangle = |\psi^{(0)}\rangle$ we calculate $|\psi(t_m = m\Delta t)\rangle = |\psi^{(m)}\rangle$ by using a generalized form of the Cayley method

$$\left(\mathbf{1} + i\delta\tilde{\boldsymbol{H}}^{(m)}\right)\frac{\mathbf{1} + i\frac{\delta}{2}\boldsymbol{U}^{(m)}}{\mathbf{1} - i\frac{\delta}{2}\boldsymbol{U}^{(m)}}|\psi^{(m+1)}\rangle = \left(\mathbf{1} - i\delta\tilde{\boldsymbol{H}}^{(m)}\right)\frac{\mathbf{1} - i\frac{\delta}{2}\boldsymbol{U}^{(m)}}{\mathbf{1} + i\frac{\delta}{2}\boldsymbol{U}^{(m)}}|\psi^{(m)}\rangle, \tag{74}$$

with $\tilde{\boldsymbol{H}}^{(m)} = \frac{1}{2}[\tilde{\boldsymbol{H}}(t_{m+1}) + \tilde{\boldsymbol{H}}(t_m)]$, $\boldsymbol{U}^{(m)} = \frac{1}{2}[\boldsymbol{U}(t_{m+1}) + \boldsymbol{U}(t_m)]$ and $\delta = \Delta t/2$. It should be noted that our propagator is norm conserving (unitary) and accurate to second-order in δ, as is the Cayley propagator.[29] Denoting by $|\psi_\alpha\rangle$ the projected wave function onto the region $\alpha = R, L, C$, we find from

Eq. (74)

$$|\psi_C^{(m+1)}\rangle = \frac{\mathbf{1}_C - i\delta \boldsymbol{H}_{\rm eff}^{(m)}}{\mathbf{1}_C + i\delta \boldsymbol{H}_{\rm eff}^{(m)}} |\psi_C^{(m)}\rangle + |S^{(m)}\rangle - |M^{(m)}\rangle. \tag{75}$$

Here, $\boldsymbol{H}_{\rm eff}^{(m)}$ is the effective Hamiltonian of the central region:

$$\boldsymbol{H}_{\rm eff}^{(m)} = \boldsymbol{H}_{CC}^{(m)} - i\delta \boldsymbol{H}_{CL} \frac{1}{\mathbf{1}_L + i\delta \boldsymbol{H}_{LL}^0} \boldsymbol{H}_{LC} - i\delta \boldsymbol{H}_{CR} \frac{1}{\mathbf{1}_R + i\delta \boldsymbol{H}_{RR}^0} \boldsymbol{H}_{RC} \tag{76}$$

with $\boldsymbol{H}_{CC}^{(m)} = \frac{1}{2}[\boldsymbol{H}_{CC}(t_{m+1}) + \boldsymbol{H}_{CC}(t_m)]$. The source term $|S^{(m)}\rangle$ describes the injection of density into the region C, while the memory term $|M^{(m)}\rangle$ is responsible for the hopping in and out of the region C. In terms of the propagator for the uncontacted and undisturbed α electrode

$$\boldsymbol{g}_\alpha = \frac{\mathbf{1}_\alpha - i\delta \boldsymbol{H}_{\alpha\alpha}^0}{\mathbf{1}_\alpha + i\delta \boldsymbol{H}_{\alpha\alpha}^0}, \tag{77}$$

the source term can be written as

$$|S^{(m)}\rangle = -\frac{2i\delta}{\mathbf{1}_C + i\delta \boldsymbol{H}_{\rm eff}^{(m)}} \sum_{\alpha=L,R} \frac{\Lambda_\alpha^{(m,0)}}{u_\alpha^{(m)}} \boldsymbol{H}_{C\alpha} \frac{[\boldsymbol{g}_\alpha]^m}{\mathbf{1}_\alpha + i\delta \boldsymbol{H}_{\alpha\alpha}^s} |\psi_\alpha^{(0)}\rangle, \tag{78}$$

with

$$u_\alpha^{(m)} = \frac{1 - i\frac{\delta}{2}U_\alpha^{(m)}}{1 + i\frac{\delta}{2}U_\alpha^{(m)}} \quad \text{and} \quad \Lambda_\alpha^{(m,k)} = \prod_{j=k}^{m} [u_\alpha^{(j)}]^2. \tag{79}$$

For a wave packet initially localized in C the projection onto the left and right electrode $|\psi_\alpha^{(0)}\rangle$ vanishes and $|S^{(m)}\rangle = 0$ for any m, as it should be. The memory term is more complicated and reads

$$|M^{(m)}\rangle = -\frac{\delta^2}{\mathbf{1}_C + i\delta \boldsymbol{H}_{\rm eff}^{(m)}} \sum_{\alpha=L,R} \sum_{k=0}^{m-1} \frac{\Lambda_\alpha^{(m,k)}}{u_\alpha^{(m)} u_\alpha^{(k)}} [\boldsymbol{Q}_\alpha^{(m-k)} + \boldsymbol{Q}_\alpha^{(m-k-1)}] \times \left(|\psi_C^{(k+1)}\rangle + |\psi_C^{(k)}\rangle\right) \tag{80}$$

where

$$\boldsymbol{Q}_\alpha^{(m)} = \boldsymbol{H}_{C\alpha} \frac{[\boldsymbol{g}_\alpha]^m}{\mathbf{1}_\alpha + i\delta \boldsymbol{H}_{\alpha\alpha}^s} \boldsymbol{H}_{\alpha C}. \tag{81}$$

The quantities $\boldsymbol{Q}_\alpha^{(m)}$ depend on the geometry of the system and are independent of the initial state $\psi^{(0)}$.

Below we propose a recursive scheme to calculate the $\boldsymbol{Q}_\alpha^{(m)}$'s for those system geometries having semiperiodic electrodes along the longitudinal direction, see

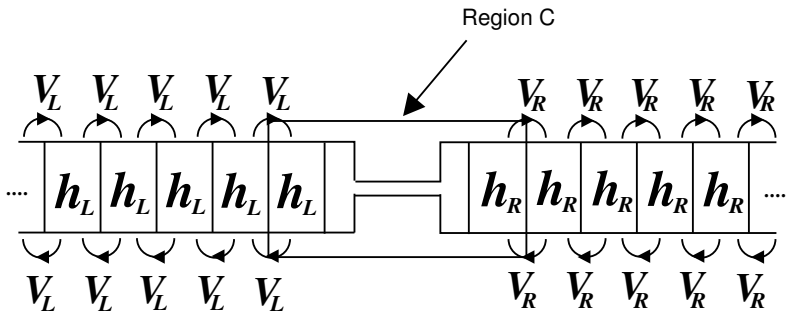

Fig. 3. Schematic sketch of an electrode-junction-electrode system with semiperiodic electrodes.

Fig. 3. In this case $\boldsymbol{H}^0_{\alpha\alpha}$ has a tridiagonal block form

$$\boldsymbol{H}^0_{\alpha\alpha} = \begin{bmatrix} \boldsymbol{h}_\alpha & \boldsymbol{V}_\alpha & 0 & \dots \\ \boldsymbol{V}_\alpha & \boldsymbol{h}_\alpha & \boldsymbol{V}_\alpha & \dots \\ 0 & \boldsymbol{V}_\alpha & \boldsymbol{h}_\alpha & \dots \\ \dots & \dots & \dots & \dots \end{bmatrix}, \tag{82}$$

where $\boldsymbol{h}_\alpha$ describes a convenient cell and $\boldsymbol{V}_\alpha$ is the hopping Hamiltonian between two nearest neighbor cells. Without loss of generality we assume that both $\boldsymbol{h}_\alpha$ and $\boldsymbol{V}_\alpha$ are square matrices of dimension $N_\alpha \times N_\alpha$. Taking into account that the central region contains the first few cells of the left and right electrodes, the matrix $\boldsymbol{Q}^{(m)}_\alpha$ has the following structure

$$\boldsymbol{Q}^{(m)}_L = \begin{bmatrix} \boldsymbol{q}^{(m)}_L & 0\ 0 \\ 0 & 0\ 0 \\ 0 & 0\ 0 \end{bmatrix}, \qquad \boldsymbol{Q}^{(m)}_R = \begin{bmatrix} 0\ 0 & 0 \\ 0\ 0 & 0 \\ 0\ 0 & \boldsymbol{q}^{(m)}_R \end{bmatrix}. \tag{83}$$

The $\boldsymbol{q}^{(m)}_\alpha$'s are square matrices of dimension $N_\alpha \times N_\alpha$ and are given by

$$\boldsymbol{q}^{(m)}_\alpha = \boldsymbol{V}_\alpha \left[\frac{[\boldsymbol{g}_\alpha]^m}{\mathbf{1}_\alpha + i\delta \boldsymbol{H}_{\alpha\alpha}} \right]_{1,1} \boldsymbol{V}_\alpha, \tag{84}$$

where the subscript $(1,1)$ denotes the first diagonal block of the matrix in the square brackets. We introduce the generating matrix function

$$\boldsymbol{q}_\alpha(x,y) \equiv \boldsymbol{V}_\alpha \left[\frac{1}{x\mathbf{1}_\alpha + iy\delta \boldsymbol{H}_{\alpha\alpha}} \right]_{1,1} \boldsymbol{V}_\alpha, \tag{85}$$

which can also be expressed in terms of continued matrix fractions

$$
\begin{aligned}
&\boldsymbol{q}_\alpha(x,y) \\
&= \boldsymbol{V}_\alpha \cfrac{1}{x+iy\delta\boldsymbol{h}_\alpha+y^2\delta^2\boldsymbol{V}_\alpha \cfrac{1}{x+iy\delta\boldsymbol{h}_\alpha+y^2\delta^2\boldsymbol{V}_\alpha \cfrac{1}{\ddots}\boldsymbol{V}_\alpha}\boldsymbol{V}_\alpha}\boldsymbol{V}_\alpha \\
&= \boldsymbol{V}_\alpha \cfrac{1}{x+iy\delta\boldsymbol{h}_\alpha+y^2\delta^2\boldsymbol{q}_\alpha(x,y)}\boldsymbol{V}_\alpha. \qquad (86)
\end{aligned}
$$

The $\boldsymbol{q}_\alpha^{(m)}$'s can be obtained from

$$
\boldsymbol{q}_\alpha^{(m)} = \frac{1}{m!}\left[-\frac{\partial}{\partial x}+\frac{\partial}{\partial y}\right]^m \boldsymbol{q}_\alpha(x,y)\Big|_{x=y=1}. \qquad (87)
$$

From Eqs. (87) and (86) one can build up a recursive scheme. Let us define $\boldsymbol{p}_\alpha^{-1}(x,y) = x+iy\delta\boldsymbol{h}_\alpha+y^2\delta^2\boldsymbol{q}_\alpha(x,y)$ and $\boldsymbol{p}_\alpha^{(m)} = \frac{1}{m!}[-\frac{\partial}{\partial x}+\frac{\partial}{\partial y}]^m\boldsymbol{p}_\alpha(x,y)|_{x=y=1}$. Then, by definition, $\boldsymbol{q}_\alpha^{(m)} = \boldsymbol{V}_\alpha\boldsymbol{p}_\alpha^{(m)}\boldsymbol{V}_\alpha$. Using the identity $\frac{1}{m!}[-\frac{\partial}{\partial x}+\frac{\partial}{\partial y}]^m\boldsymbol{p}_\alpha(x,y)\boldsymbol{p}_\alpha^{-1}(x,y)=0$, one finds

$$
(1+i\delta\boldsymbol{h}_\alpha)\boldsymbol{p}_\alpha^{(m)} = (1-i\delta\boldsymbol{h}_\alpha)\boldsymbol{p}_\alpha^{(m-1)} - \delta^2\sum_{k=0}^{m}(\boldsymbol{q}_\alpha^{(k)}+2\boldsymbol{q}_\alpha^{(k-1)}+\boldsymbol{q}_\alpha^{(k-2)})\boldsymbol{p}_\alpha^{(m-k)} \qquad (88)
$$

with $\boldsymbol{p}_\alpha^{(m)} = \boldsymbol{q}_\alpha^{(m)} = 0$ for $m<0$. Once $\boldsymbol{q}_\alpha^{(0)}$ has been obtained by solving Eq. (86) with $x=y=1$, we can calculate $\boldsymbol{p}_\alpha^{(0)} = [1+i\delta\boldsymbol{h}_\alpha+\delta^2\boldsymbol{q}_\alpha^{(0)}]^{-1}$. Afterwards, we can use Eq. (88) with $\boldsymbol{q}_\alpha^{(1)} = \boldsymbol{V}_\alpha\boldsymbol{p}_\alpha^{(1)}\boldsymbol{V}_\alpha$ to calculate $\boldsymbol{p}_\alpha^{(1)}$ and hence $\boldsymbol{q}_\alpha^{(1)}$ and so on and so forth.

This concludes the description of our algorithm for the propagation of the time-dependent Schrödinger equation for extended systems. It is worth mentioning an additional complication here which arises for the propagation of a time-dependent Kohn-Sham equation. This complication stems from the fact that in order to compute $|\psi_C^{(m+1)}\rangle$ at time step $m+1$ one needs to know the time-dependent KS potential at the same time step which, via the Hartree and exchange-correlation potentials, depends on the yet unknown orbitals $|\psi_C^{(m+1)}\rangle$. Of course, the solution is to use a predictor-corrector approach: in the first step one approximates $\boldsymbol{H}_{CC}^{(m)}$ by $\boldsymbol{H}_{CC}(t_m)$, computes new orbitals $|\tilde{\psi}_C^{(m+1)}\rangle$ and from those obtains an improved approximation for $\boldsymbol{H}_{CC}^{(m)}$.

5 Implementation details for 1d systems and numerical results

All the methodological discussion of Section 4 is general and can be applied to all systems having a longitudinal geometry like the one in Fig. 3. In this Section we show that the proposed scheme is feasible by testing it against

one-dimensional model systems. The extension to real molecular-device configurations is presently under development [30]. We consider systems described by the Hamiltonian

$$\langle x|\boldsymbol{H}|x'\rangle = \delta(x-x')\left[-\frac{1}{2}\frac{\mathrm{d}}{\mathrm{d}x^2}+V(x)\right]. \tag{89}$$

We have used a simple three-point discretization for the second derivative

$$\frac{\mathrm{d}^2}{\mathrm{d}x^2}\psi(x)|_{x=x_i} \approx \frac{1}{(\Delta x)^2}\left[\psi(x_{i+1})-2\psi(x_i)+\psi(x_{i-1})\right] \tag{90}$$

with equidistant grid points x_i, $i=1,\ldots,N_g$ and spacing Δx. Within this approximation matrices of the form $\boldsymbol{H}_{C\alpha}\boldsymbol{M}\boldsymbol{H}_{\alpha C}$ which are $N_g \times N_g$ matrices and appear, e.g., in Eq. (38) or (81), have only one nonvanishing matrix element. For $\alpha = L$ this is the $(1,1)$ element, for $\alpha = R$ it is the (N_g, N_g) element.

In order to proceed we have to specify the nature of the leads and therefore the lead Green function. Here we choose the simplest case of semi-infinite, uniform leads at constant potential $U_{\alpha 0}$. In this case, the retarded Green function $\boldsymbol{g}^{\mathrm{R}}_{\alpha\alpha}$ in the energy domain can be given in closed form:

$$\begin{aligned}[\boldsymbol{g}^{\mathrm{R}}_{\alpha\alpha}(E)]_{kl} = &-\frac{i\Delta x}{\sqrt{2\tilde{E}_\alpha}}\exp\left\{i\sqrt{2\tilde{E}_\alpha}|x_k-x_l|\right\} \\ &+\frac{i\Delta x}{\sqrt{2\tilde{E}_\alpha}}\exp\left\{i\sqrt{2\tilde{E}_\alpha}(|x_k-x_{\alpha 0}|+|x_l-x_{\alpha 0}|)\right\}\end{aligned} \tag{91}$$

with $\tilde{E}_\alpha = E - U_{\alpha 0}$. The abscissa $x_{\alpha 0}$ is the position of the interface between the lead and the device region; in our implementation x_{L0} is the first grid point of region C while x_{R0} is the N_g-th grid point of region C. According to the notation in Eq. (63) the one-particle state of region C describing an electron localized in x_{L0} is denoted by $|x_{C1}\rangle$ while the one-particle state of region C describing an electron localized in x_{R0} is denoted by $|x_{CN_g}\rangle$. The coordinate $x_k = x_{\alpha 0} \pm k\Delta x$, $k>0$, where the plus sign applies for $\alpha = R$ and the minus sign for $\alpha = L$.

The results of the procedure for calculating extended eigenstates as described in Section 4.1 is illustrated in Fig. 4 for a square potential barrier with zero potential in both leads. In the left panel we have the square modulus of eigenstates at an energy below the barrier height while in the right panel eigenstates with energy higher than the barrier are shown. The states result from diagonalization of Eq. (71). In order to obtain the normalization constant we compute the logarithmic derivative at the boundary of the central region numerically

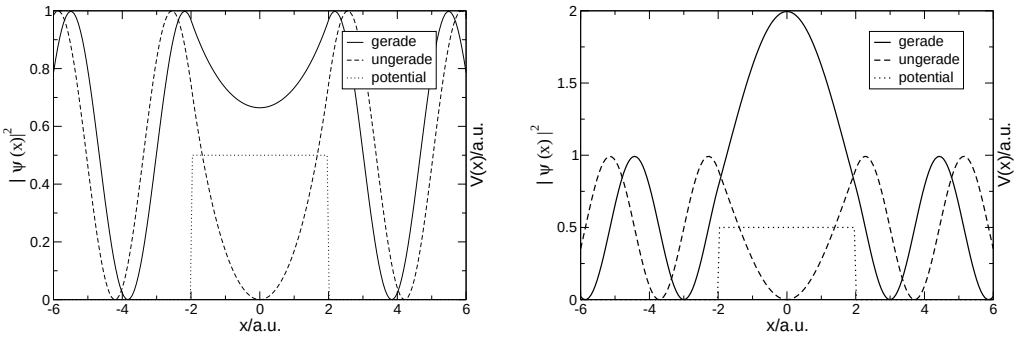

Fig. 4. Continuum states of square potential barrier at different energies with leads at zero potential. Left panel: eigenstates for $\varepsilon = 0.45$ a.u., just below the barrier height of 0.5 a.u.. Right panel: eigenstates at $\varepsilon = 0.6$ a.u..

and match it to the analytic form in the lead to obtain the phase shift δ_α:

$$\frac{1}{2}\frac{\mathrm{d}^2}{\mathrm{d}x^2}\ln(|\psi(x)|^2)\bigg|_{x=x_{\alpha 0}} = q\cot(\delta_\alpha) \tag{92}$$

where $q = \sqrt{2\tilde{E}_\alpha}$. Knowing the phase shift we can rescale the wavefunction such that it matches with the analytic form $\sin(q(x-x_{\alpha 0})+\delta_\alpha)$ at the interface. Of course, this form of the extended states only applies for $\tilde{E}_\alpha > 0$ but as long as E is in the continuous part of the spectrum, it is correct at least for one of the leads. This is sufficient to determine the normalization. The states obtained numerically with this procedure coincide with the known analytical results.

We then implemented the propagation scheme presented in the previous Section. Within our three-point approximation, $\boldsymbol{h}_\alpha$, $\boldsymbol{V}_\alpha$ and $\boldsymbol{q}_\alpha$ are 1×1 matrices. The equation for $q_\alpha^{(0)}$ [see Eqs. (86) and (87)] becomes a simple quadratic equation which can be solved explicitly

$$q_\alpha^{(0)} = \frac{-(1+i\delta h_\alpha) + \sqrt{(1+i\delta h_\alpha)^2 + 4(\delta V_\alpha)^2}}{2\delta^2}\,. \tag{93}$$

Although the quadratic equation has two solutions, the above choice for $q_\alpha^{(0)}$ is dictated by the fact that the Taylor expansions for small δ of Eqs. (93) and (86) have to coincide. Using this result we then solved the iterative scheme to obtain the $q_\alpha^{(m)}$ for $m \geq 1$.

As a first check on the propagation method we propagated a Gaussian wavepacket which, at initial time $t = 0$, is completely localized in the central device region. (The source terms $|S^{(m)}\rangle$ then vanish identically). As can be seen in Fig. 5, the wavepacket correctly propagates through the boundaries without any spurious reflections.

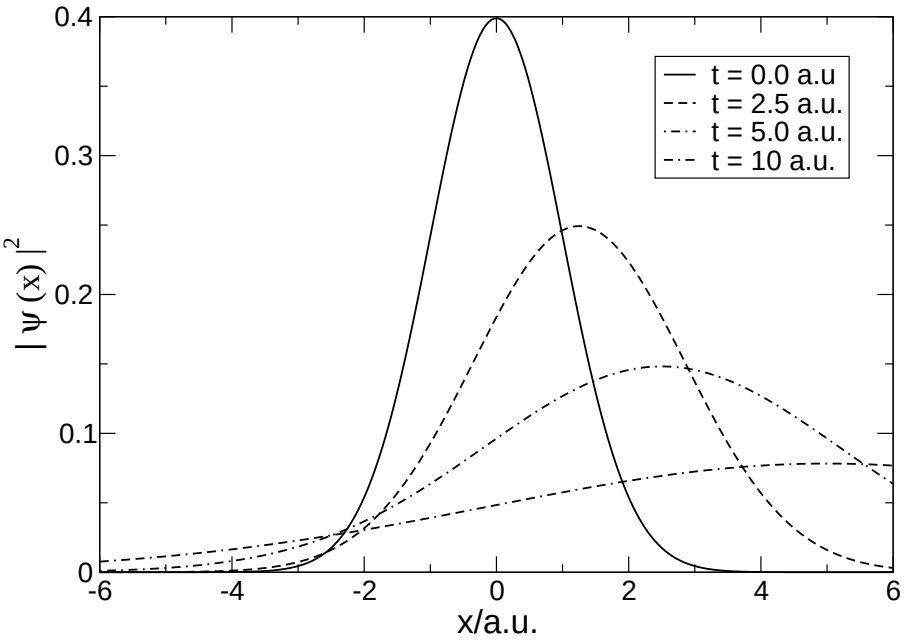

Fig. 5. Time evolution of a Gaussian wavepacket with initial width 1.0 a.u. and initial momentum 0.5 a.u. for various propagation times. The transparent boundary conditions allow the wavepacket to pass the propagation region without spurious reflections at the boundaries.

For the propagation of the extended initial states (the eigenstates of the unperturbed system) we also need to implement the source terms $|S^{(m)}\rangle$. In the following we assume that the left and right leads are at the same potential initially so that the analytic form of the initial states is in both leads given by $\sin(q(x-x_{\alpha 0})+\delta_\alpha) = [\exp(i\delta_\alpha - iqx_{\alpha 0})\exp(iqx) - \text{c.c.}]/2i$. Let us specialize the discussion to the case $\alpha = R$ and define the state $|q_R\rangle$ according to $\langle x_{Rk}|q_R\rangle = \exp(iqk\Delta x)$, where $|x_{Rk}\rangle$ is the one-particle state of electrode R describing an electron localized in $x_k = x_{R0} + k\Delta x$, $k > 0$. Then, the projection of the initial state onto lead R reads $|\psi_R^{(0)}\rangle = \frac{1}{2i}[\exp(i\delta_\alpha)|q_R\rangle - \exp(-i\delta_\alpha)|-q_R\rangle]$. From Eq. (78) the contribution to the source term for $\alpha = R$ is completely known once we know how $\boldsymbol{H}_{CR}[\boldsymbol{g}_R]^m/(\mathbf{1}_R + i\delta\boldsymbol{H}_{RR})$ acts on the state $|q_R\rangle$. We have

$$\boldsymbol{H}_{CR}\frac{[\boldsymbol{g}_R]^m}{(\mathbf{1}_R + i\delta\boldsymbol{H}_{RR})}|q_R\rangle = V_R|x_{CN_g}\rangle\langle x_{R1}|\frac{[\boldsymbol{g}_R]^m}{(\mathbf{1}_R + i\delta\boldsymbol{H}_{RR})}|q_R\rangle \qquad (94)$$

where x_{CN_g} corresponds the N_g-th discretization point of region C (the last point on the right before electrode R starts). We rewrite the unknown quantity as follows

$$\langle x_{R1}|\frac{[\boldsymbol{g}_R]^m}{\mathbf{1}_R + i\delta\boldsymbol{H}_{RR}}|q_R\rangle = \frac{[D(x,y)]^m}{m!}\rho(x,y)\Big|_{x=y=1}, \qquad (95)$$

with

$$D(x,y)=\left(-\frac{\partial}{\partial x}+\frac{\partial}{\partial y}\right),\quad \rho(x,y)=\langle x_{R1}|\frac{1}{x\mathbf{1}_R+iy\delta\boldsymbol{H}_{RR}}|q_R\rangle. \tag{96}$$

Next, we use the Dyson equation to find an explicit expression for $\rho(x,y)$. We have

$$\frac{1}{x\mathbf{1}_R+iy\delta\boldsymbol{H}_{RR}}|q_R\rangle=\frac{1}{x}|q_R\rangle-\frac{1}{x}\frac{iy\delta}{x\mathbf{1}_R+iy\delta\boldsymbol{H}_{RR}}\boldsymbol{H}_{RR}|q_R\rangle. \tag{97}$$

It is straightforward to realize that the action of $\boldsymbol{H}_{RR}$ on $|q_R\rangle$ yields

$$\boldsymbol{H}_{RR}|q_R\rangle=(2V_R\cos(q\Delta x)+h_R)|q_R\rangle-V_R\mathrm{e}^{-iq\Delta x}|x_{R1}\rangle, \tag{98}$$

so that Eq. (97) can be rewritten as

$$\left[1+\frac{2iy\delta V_R\cos(q\Delta x)+iy\delta h_R}{x}\right]\frac{1}{x\mathbf{1}_R+iy\delta\boldsymbol{H}_{RR}}|q_R\rangle= \frac{1}{x}|q_R\rangle+\frac{1}{x}\frac{iy\delta V_R\mathrm{e}^{-iq\Delta x}}{x\mathbf{1}_R+iy\delta\boldsymbol{H}_{RR}}|x_{R1}\rangle. \tag{99}$$

Projecting Eq. (99) on $\langle x_{R0}|$ we find

$$\left[1+\frac{2iy\delta V_R\cos(q\Delta x)+iy\delta h_R}{x}\right]\rho(x,y)=\frac{1}{x}+\frac{iy\delta\mathrm{e}^{-iq\Delta x}}{xV_R}q_R(x,y), \tag{100}$$

where $q_R(x,y)$ is the generating function defined in Eq. (85). Solving Eq. (100) for $\rho(x,y)$ we conclude that

$$V_R\rho(x,y)=\frac{V_R+iy\delta\mathrm{e}^{-iq\Delta x}q_R(x,y)}{x+2iy\delta V_R\cos(q\Delta x)+iy\delta h_R}. \tag{101}$$

Using the relation in Eq. (87) for the coefficients $q_\alpha^{(m)}$ we find

$$\frac{[D(x,y)]^m}{m!}\rho(x,y)\Big|_{x=y=1}=\frac{(1-(2i\delta V_R\cos(q\Delta x)+i\delta h_R))^m}{(1+(2i\delta V_R\cos(q\Delta x)+i\delta h_R))^{m+1}}+\frac{i\delta}{V_R}\mathrm{e}^{-iq\Delta x} \times\sum_{j=0}^{m}\frac{(1-(2i\delta V_R\cos(q\Delta x)+i\delta h_R))^{m-j}}{(1+(2i\delta V_R\cos(q\Delta x)+i\delta h_R))^{m+1-j}}\left(q_R^{(j)}+q_R^{(j-1)}\right). \tag{102}$$

One may proceed along the same lines for extracting the left component of the source term.

To test our implementation we have propagated eigenstates of the extended system. As expected, these states just pick up an exponential phase factor $\exp(-iEt)$ during the propagation.

We are now in a position to apply our algorithm to the calculation of time-dependent currents in one-dimensional model systems. The systems are initially in thermodynamic equilibrium. At time $t = 0$, a time-dependent perturbation is switched on. In all the examples below the current is calculated according to Eq. (62)

$$\begin{aligned} I(x,t) &= 2\int_{-k_F}^{k_F} \frac{\mathrm{d}k}{2\pi}\,\mathrm{Im}\,\left(\psi_k^*(x,t)\frac{\mathrm{d}}{\mathrm{d}x}\psi_k(x,t)\right) \\ &= 2\int_{0}^{k_F} \frac{\mathrm{d}k}{2\pi}\,\mathrm{Im}\,\left(\psi_k^*\frac{\mathrm{d}}{\mathrm{d}x}\psi_k + \psi_{-k}^*\frac{\mathrm{d}}{\mathrm{d}x}\psi_{-k}\right) \end{aligned} \tag{103}$$

where the prefactor 2 comes from spin and $k_F = \sqrt{2\varepsilon_F}$ is the Fermi wavevector of a system with Fermi energy ε_F.

5.1 DC bias

As a first example we considered a system where the electrostatic potential vanishes identically both in the left and right leads as well as in the central region which is explicitly propagated. Initially, all single particle levels are occupied up to the Fermi energy ε_F. At $t = 0$ a constant bias is switched on in the leads and the time-evolution of the system is calculated. We chose the bias in the right lead as the negative of the bias in the left lead, $U_R = -U_L$.

The numerical parameters are as follows: the Fermi energy is $\varepsilon_F = 0.3$ a.u., the bias is $U_L = -U_R = 0.05$, 0.15, 0.25 a.u., the central region extends from $x = -6$ to $x = +6$ a.u. with equidistant grid points with spacing $\Delta x = 0.03$ a.u.. The k-integral in Eq. (103) is discretized with 100 k-points which amounts to a propagation of 200 states. The time step for the propagation was $\Delta t = 10^{-2}$ a.u.

In Fig. 6 we have plotted the current densities at $x = 0$ as a function of time for different values of the applied bias. As a first feature we notice that a steady state is achieved, in agreement with the discussion of Section 3.3. The corresponding steady-state current $I^{(\mathrm{S})}$ can be calculated from the Landauer formula. For the present geometry this leads to the steady current

$$\begin{aligned} I^{(\mathrm{S})} = 8e\int_{\max(U_L,U_R)} & \frac{d\omega}{2\pi}[f(\omega-U_L)-f(\omega-U_R)] \\ & \times \frac{\sqrt{\omega-U_L}\sqrt{\omega-U_R}}{\left[\sqrt{\omega-U_L}+\sqrt{\omega-U_R}\right]^2 + U_L U_R\left[\dfrac{\sin(l\sqrt{2\omega})}{\sqrt{\omega}}\right]^2}, \end{aligned} \tag{104}$$

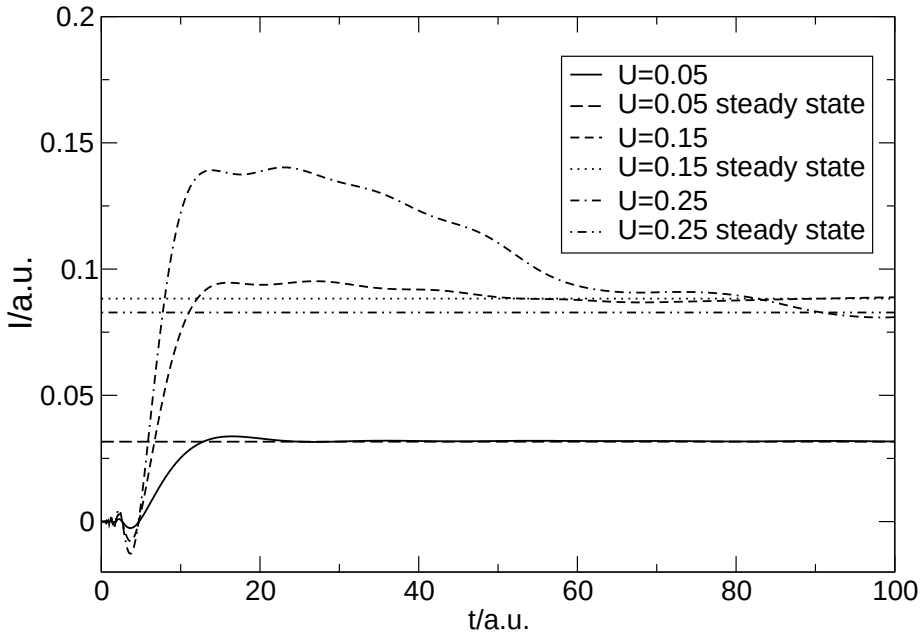

Fig. 6. Time evolution of the current for a system where initially the potential is zero in the leads and the propagation region. At $t = 0$, a constant bias with opposite sign in the left and right leads is switched on, $U = U_L = -U_R$ (values in atomic units). The propagation region extends from $x = -6$ to $x = +6$ a.u.. The Fermi energy of the initial state is $\varepsilon_F = 0.3$ a.u.. The current in the center of the propagation region is shown.

where l is the width of the central region. From Eq. (104) with $l = 12$ a.u. and $U_L = -U_R$, the numerical values for the steady-state currents are 0.0316 a.u. ($U_L = 0.05$ a.u.), 0.0883 a.u. ($U_L = 0.15$ a.u.) and 0.0828 a.u. ($U_L = 0.25$ a.u.). We see that our algorithm yields the same answers. Second, we notice that the onset of the current is delayed in relation to the switching time $t = 0$. This is easily explained by the fact that the perturbation at $t = 0$ happens in the leads only, *e.g.*, for $|x| > 6$ a.u., while we plot the current at $x = 0$. In other words, we see the delay time needed for the perturbation to propagate from the leads to the center of our device region. We also note that the higher the bias the more the current overshoots its steady-state value for small times after switching on the bias. Finally it is worth mentioning that increasing the bias not necessarily leads to a larger steady-state current.

In the second example we studied a double square potential barrier with electrostatic potential $V(x) = 0.5$ a.u. for 5 a.u. $\leq |x| \leq 6$ a.u. and zero otherwise. This time we switch on a constant bias in the left lead only, *i.e.*, $U_R = 0$. The Fermi energy for the initial state is $\varepsilon_F = 0.3$ a.u.. The central region extends from $x = -6$ to $x = +6$ a.u. with a lattice spacing of $\Delta x = 0.03$ a.u.. Again, we use 100 different k-values to compute the current and a time step of $\Delta t = 10^{-2}$ a.u..

In Fig. 7 (Left panel) we plot the current at $x = 0$ as a function of time for

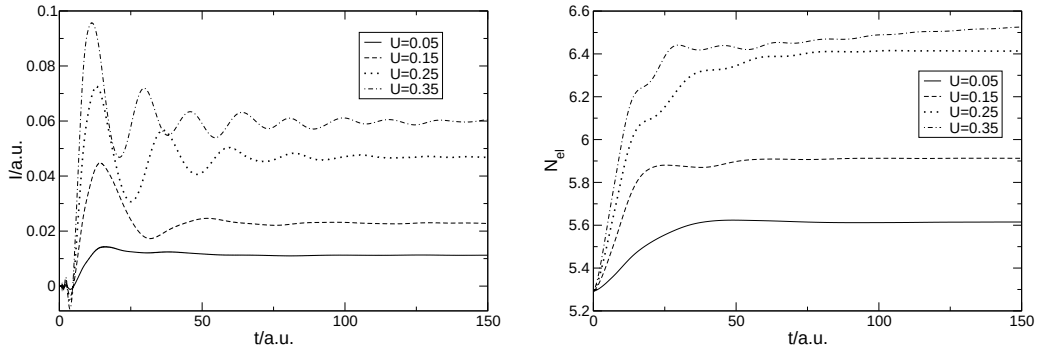

Fig. 7. Left panel: Time evolution of the current through a double square potential barrier in response to an applied constant bias (given in atomic units) in the left lead. The potential is given by $V(x) = 0.5$ a.u. for $5 \leq |x| \leq 6$ a.u. and zero otherwise, the propagation region extends from $x = -6$ to $x = +6$ a.u.. The Fermi energy of the initial state is $\varepsilon_F = 0.3$ a.u.. The current in the center of the structure is shown. Right panel: Time evolution of the total number of electrons in the region $|x| \leq 6$ for the same double square potential barrier.

several values of the applied bias $U = U_L$. Again, a steady state is achieved for all values of U. As discussed in Fig. 6 the transient current can exceed the steady current; the higher the applied voltage the larger is this excess current and the shorter is the time when it reaches its maximum. Furthermore, the oscillatory evolution towards the steady current solution depends on the bias. For high bias the frequency of the transient oscillations increases. For small bias the electrons at the bottom of the band are not disturbed and the transient process is exponentially short. On the other hand, for a bias close to the Fermi energy the transient process decays as a power law, due to the band edge singularity. As pointed out in Section 3.3, for non-interacting electrons the steady-state current develops by means of a pure dephasing mechanism. In our examples the transient process occurs in a femtosecond time-scale, which is much shorter than the relaxation time due to electron-phonon interactions.

In Fig. 7 (Right panel) we plot the time evolution of the total number of electrons in the device region for the same values of U_L. We see that as a result of the bias a quite substantial amount of charge is added to the device region. This result has important implications when simulating the transport through an interacting system as the effective (dynamical) electronic screening is modified due not only to the external field but also to the accumulation of charge state in the molecular device. This illustrates that linear response might not be an appropriate tool to tackle the dynamical response and that we will need to resort to a full time-propagation approach as the one presented in this review. Here we emphasize that all our calculations are done without taking into account the electron-electron interaction. If we had done a similar calculation with the interaction incorporated in a time-dependent Hartree or time-dependent DFT framework we would expect the amount of excess charge

to be reduced significantly as compared to Fig. 7.

5.2 Time-dependent biases

In the previous Section we have shown how a steady current develops after the switching on of a constant bias and discussed the transient regime. Here we exploit the versatility of our proposed algorithm for studying different kinds of time-dependent biases.

As a first example we consider how the current responds to a sudden switching off of the bias. For comparison we have considered the same double square potential barrier of Fig. 7 subject to the same suddenly switched on bias, but we have turned off the bias at $t = 75$ a.u. The results (obtained with the same parameters of Fig. 7) are displayed in Fig. 8. We observe that the current shows a rather well pronounced peak shortly after switching off the perturbation. The amplitude of the peak is proportional to the originally applied bias. This peak always overshoots the value of the current at the steady state. Another interesting feature is the fact that after turning off the bias the transient currents show only two oscillations around the zero current limit and the transient time for switching off is much shorter than for switching on a high bias.

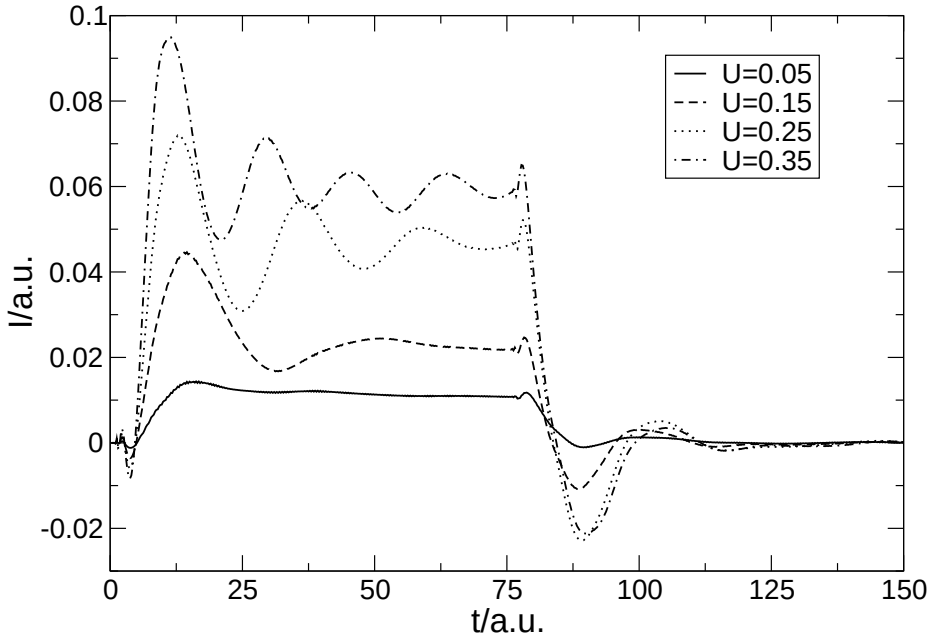

Fig. 8. Same system of Fig. 7 exposed to a suddenly switched on bias at $t = 0$. The bias is then turned off at $t = 75$ a.u. The current is measured in the middle of the central region.

We have also addressed the simulation of AC-transport. We computed the

current for a single square potential barrier with $V(x) = 0.6$ for $|x| < 6$ and zero otherwise. Here we applied a time-dependent bias of the form $U_L(t) = U_0 \sin(\omega t)$ to the left lead. The right lead remains on zero bias. The numerical parameters are: Fermi energy $\varepsilon_F = 0.5$ a.u., device region from $x = -6$ to $x = +6$ a.u. with lattice spacing $\Delta x = 0.03$ a.u.. The number of k-points is 100 and the time step is $\Delta t = 10^{-2}$ a.u.. In Fig. 9 we plot the current at $x = 0$ as a function of time for different values of the parameter $U_0 = 0.1, 0.2, 0.3$ a.u. The frequency was chosen as $\omega = 1.0$ a.u. in both cases. Again, as for the DC-calculation discussed above, we get a transient that overshoots the average current flowing through the constriction; again, this excess current is larger the higher the applied voltage. Also, after the transient we obtain a current through the system with the same period as the applied bias. Note, however, that (especially for the large bias), the current is not a simple harmonic as the applied AC bias.

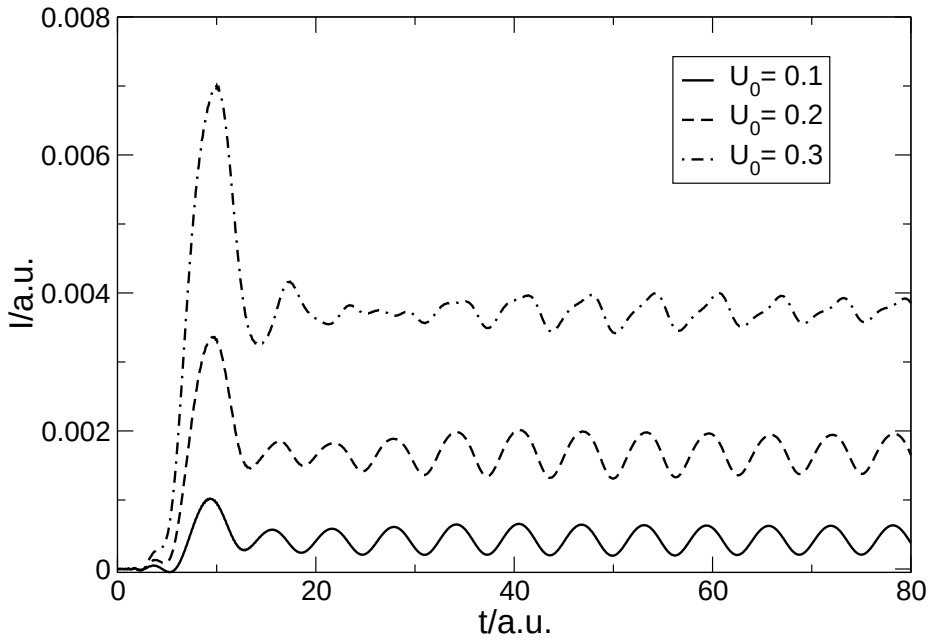

Fig. 9. Time evolution of the current for a square potential barrier in response to a time-dependent, harmonic bias in the left lead, $U_L(t) = U_0 \sin(\omega t)$ for different amplitudes U_0 (values in a.u.) and frequency $\omega = 1.0$ a.u.. The potential is given by $V(x) = 0.6$ a.u. for $|x| \leq 6.0$ a.u. and zero otherwise. The propagation region extends from $x = -6$ to $x = +6$ a.u.. The Fermi energy of the initial state is $\varepsilon_F = 0.5$ a.u.. The current at $x = 0$ is shown.

Exposing the system to an AC bias also allows us to acquire information about the excitation energies of the molecular device. In Fig. 10 (Left panel) we plot the time dependent current for a symmetric double square potential barrier in response to a harmonic bias in the left lead, $U_L(t) = U_0 \sin(\omega t)$, with $U_0 = 0.15$ a.u. and $\omega = 0.03$ a.u.. The Fermi energy of the initial state is $\varepsilon_F = 0.3$ a.u. and the current at $x = 0$ is shown. The central region extends from $x = -6$ to $x = 6$ a.u. with lattice spacing $\Delta x = 0.03$ a.u. and the

potential $V(x)$ in region C is given by $V(x) = 0$ for $|x|/\text{a.u.} < (6-d)$ and $V(x) = 0.5$ a.u. for $(6-d) < |x|/\text{a.u.} < 6$. The number of k-points is 100 and the time step is $\Delta t = 10^{-2}$ a.u.. We have studied barriers of different thickness $d = 1$ a.u. and $d = 2$ a.u.. For $d = 2$ a.u. we observe small oscillations superimposed to the oscillations of frequency $\omega = 0.03$ a.u. driven by the external AC field. Such small oscillations have frequency $\simeq 0.23$ and can be understood by looking at the transmission function $T(E)$ in the Right panel of Fig. 10. For $d = 2$ a.u. both the second and third peaks of $T(E)$ are in the energy window $(\varepsilon_F - U_0, \varepsilon_F + U_0) = (0.15, 0.45)$ a.u.. The energy difference between these two peaks corresponds to a good extent to the frequency of the superimposed oscillations. On the contrary, for $d = 1$ a.u. only one peak of the transmission function $T(E)$ is contained in the aforementioned energy window and no superimposed oscillations are clearly visible. This example shows the AC quantum transport can be used also for probing molecular devices.

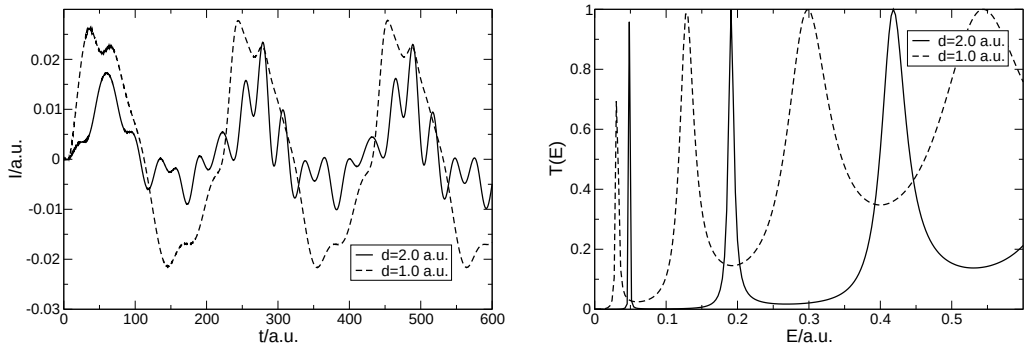

Fig. 10. Left panel: Time evolution of the current for a symmetric double square potential barrier in response to a time-dependent, harmonic bias in the left lead, $U_L(t) = U_0 \sin(\omega t)$ with $U_0 = 0.15$ a.u. and $\omega = 0.03$ a.u. for different thickness $d = 1$ and $d = 2$ a.u. of the barriers. Right Panel: Transmission function of the same double square potential barrier for $d = 1$ and $d = 2$ a.u.

5.3 History dependence

In Fig. 11 we show time-dependent currents for the same double barrier as in Fig. 7 for two different ways of applying the bias in the left lead: in one case the constant bias U_0 is switched on suddenly at $t = 0$ (as in Fig. 7), in the other case the constant U_0 is achieved with a smooth switching $U(t) = U_0 \sin^2(\omega t)$ for $0 < t < \pi/(2\omega)$. As expected and in agreement with the results of Section 3.3, the same steady state is achieved after the initial transient time. However, the transient current clearly depends on how the bias is switched on.

According to the result in Eq. (39), for noninteracting electrons the independence of the history is not limited to steady-state regimes. The long-time behaviour of currents $I(t)$ and $I'(t)$ induced by biases $U_\alpha(t)$ and $U'_\alpha(t)$ does

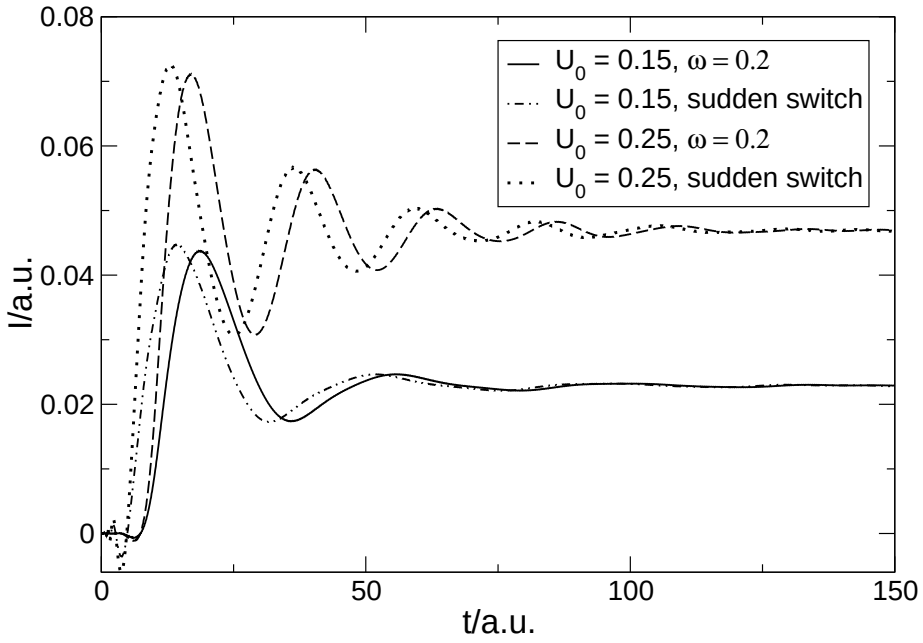

Fig. 11. Time evolution of the current for a double square potential barrier when the bias is switched on in two different manners: in one case, the bias U_0 is suddenly switched on at $t = 0$ while in the other case the same bias is achieved with a smooth switching $U(t) = U_0 \sin^2(\omega t)$ for $0 < t < \pi/(2\omega)$. The parameters for the double barrier and the other numerical parameters are the same as the ones used in Fig. 7. U_0 and ω given in atomic units.

not change provided $U_\alpha - U'_\alpha \to 0$ for $t \to \infty$. For instance, the current response to an AC bias has the same periodic modulation and the *same phase* independently of how the AC bias is switched on. In Fig. 12 we plot the time-dependent current for the same system (and using the same parameters) of Fig. 9. The bias remains on zero in the right lead. In the left lead we applied a time-dependent bias of the form $U_L(t) = U_0 f(t) \sin(\omega t)$, with $U_0 = 0.2$ a.u., $\omega = 1.0$ a.u., and we considered two different "switching on" functions $f(t)$. The first is $f(t) = 1$ (as in Fig. 9) while the second is a ramp-like switching-on $f(t) = \theta(T-t)t/T + \theta(t-T)$ with $T = 30$ a.u.. As expected, and in agreement with Eq. (39), the current has the same behaviour in the long-time limit.

5.4 Pumping current: preliminary results

Our algorithm is also well-suited to study pumping of electrons. An electron pump is a device which generates a DC current between two electrodes kept at the same bias. The pumping is achieved by applying a periodic gate voltage depending on two or more parameters. Electron pumps have been realized experimentally, e.g., for an open semiconductor quantum dot [31] where pumping was achieved by applying two harmonic gate voltages with a phase shift.

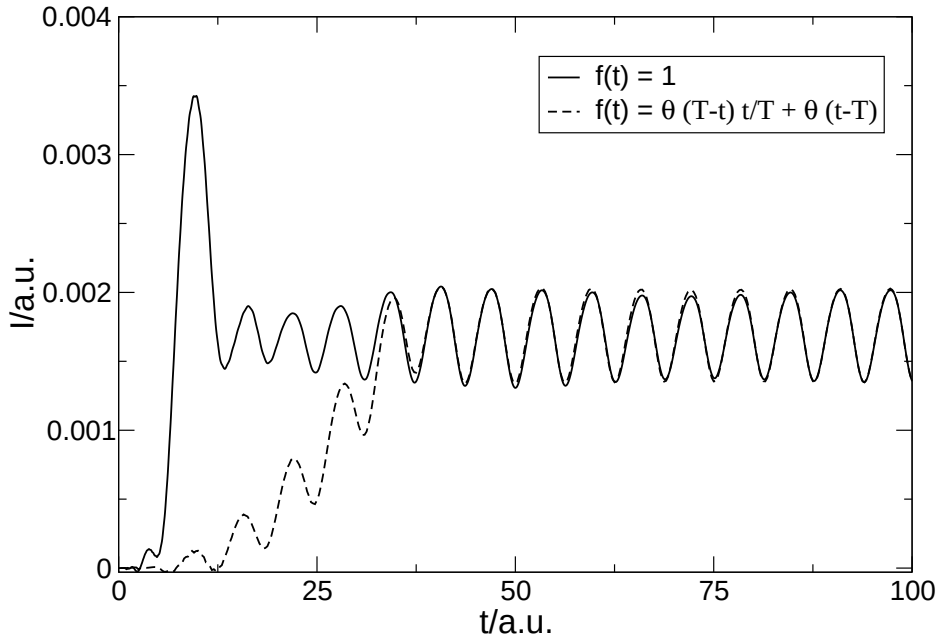

Fig. 12. Time evolution of the current for a square potential barrier in response to a time-dependent, harmonic bias in the left lead, $U_L(t) = U_0 f(t) \sin(\omega t)$ with $U_0 = 0.2$ a.u. and frequency $\omega = 1.0$ a.u.. The system and the parameters used are the same as in Fig. 9. The current at $x = 0$ is shown for two different "switching on" functions $f(t)$.

In the literature, different techniques have been used to discuss electron pumping theoretically. Brouwer [32] suggested a scattering approach to describe pumping of non-interacting electrons which has been used, e.g., to study pumping through a double barrier [33]. Nonequilibrium Green's function techniques have been used to study pumping in tight-binding models of coupled quantum dots [34]. Alternatively, Floquet theory which describes evolution of a quantum system under the influence of time-periodic fields is also well-suited to describe pumping [35].

As a first example of electron pumping we have calculated the time evolution of the density for a single square barrier exposed to a travelling potential wave $U(t) = U_0 \sin(qx - \omega t)$. The wave is spatially restricted to the explicitly treated device region which in our case also coincides with the static potential barrier. Some snapshots of the density and the potential wave are shown in Fig. 13. The density in the device region clearly exhibits local maxima in the potential minima and is transported in pockets by the wave. This is also evident in Fig. 14 where we show the time-dependent density as function of both position and time throughout the propagation. The density contour lines show transport of electrons from the left lead at $x = -8$ to the right lead at $x = +8$ a.u.. The pumping mechanism in this example resembles pumping of water with the Archimedean screw.

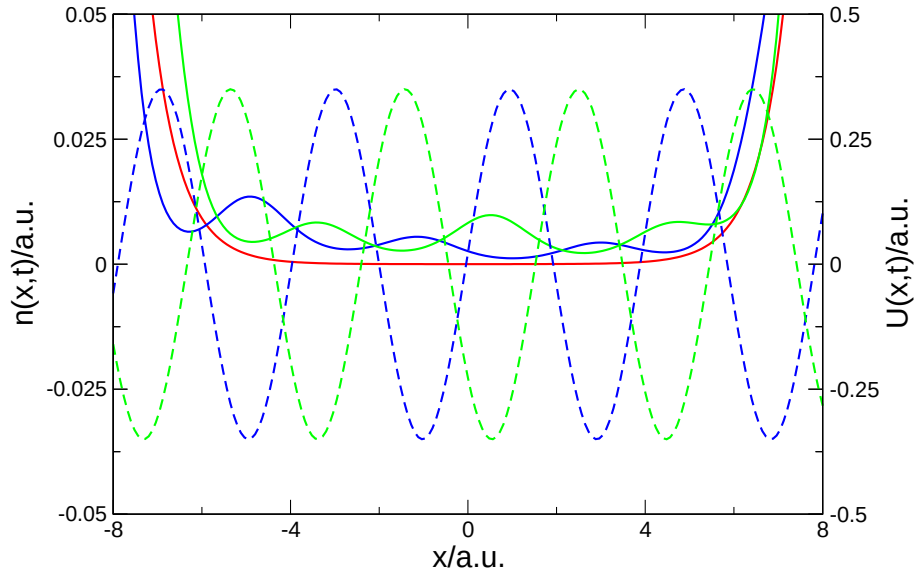

Fig. 13. Snapshots of the density for and the travelling potential wave at various times for pumping through a single square barrier by a travelling wave. The barrier with height 0.5 a.u. extends throughout the propagation window from $x = -8$ to $x = +8$. The leads are on zero potential and the Fermi level is at 0.3 a.u.. The travelling potential wave is restricted to the propagation window $|x| < 8$ and has the form $U(t) = U_0 \sin(qx - \omega t)$ with amplitude $U_0 = 0.35$ a.u., wave number $q = 1.6$ a.u. and frequency $\omega = 0.2$ a.u.. The initial density is given by the red line.

As a second example we have calculated pumping through a double square barrier by applying two harmonic gate voltages with a phase difference to the barrier potentials, i.e., $U(x,t) = U_0 \sin(\omega t)$ for the left barrier and $U(x,t) = U_0 \sin(\omega t + \phi)$ for the right barrier. Fig. 15 shows the DC component of the pump current as a function of the phase ϕ which has a sinusoidal dependence for our parameter values. This is in agreement with similar results of Ref. [33] for small amplitudes of the AC bias which were obtained using Brouwer's approach. In addition, this example may be interpreted as a very simple model to describe the experiment of Ref. [31].

6 Conclusions and perspectives

In this review we have given a self-contained introduction to our recent approach to quantum transport. In essence our approach combines two well-established theories for the description of non-equilibrium phenomena of interacting many-electron systems.

On the one hand there is the formalism of non-equilibrium Keldysh-Green functions. Although this approach in principle can be used to study interaction effects, here we only used it in the context of non-interacting electrons. The

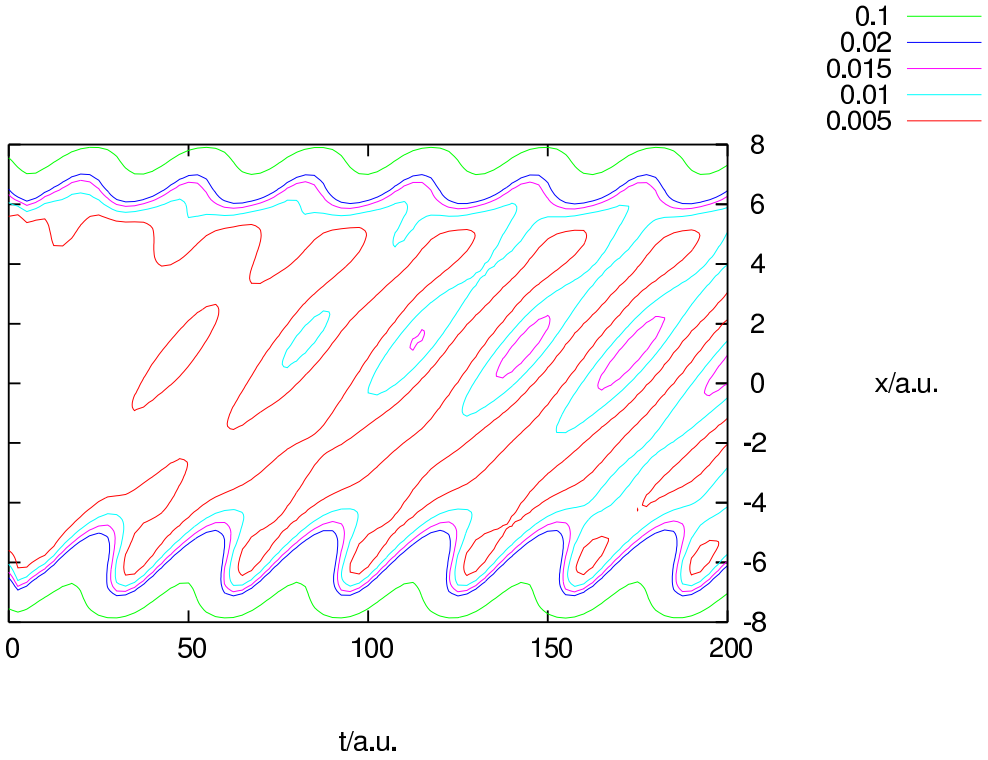

Fig. 14. Contour plot of the time-dependent density for pumping through a single square barrier by a travelling potential wave. The parameters are the same as for Fig. 13.

reason for this is that the self-energy of interacting electrons (which is not to be confused with the embedding self-energy) is long-range and nonlocal. In our scheme which partitions space in left and right leads as well as the central device region, this non-locality is extremely difficult to deal with in a rigorous manner.

On the other hand, the NEGF formalism for (effectively) non-interacting electrons can easily be combined with the second approach for time-dependent many-particle systems, namely time-dependent density functional theory. Just as the NEGF formalism, TDDFT in principle gives the correct time-dependent density of the interacting system (if the exact exchange-correlation potential is used). Moreover, the time-dependent effective single-particle potential of TDDFT is a local and multiplicative potential which is crucial for practical use within the partitioning scheme for transport.

In combining the NEGF and TDDFT approaches we have presented a formally rigorous approach towards the description of charge transport using an open-boundary scheme within TDDFT. We have implemented a specific time-propagation scheme that incorporates transparent boundaries at the device/lead interface in a natural way. In order to have a clear definition of a device region in Fig. 1 we assumed that an applied bias can be described by adding a spatially constant potential shift in the macroscopic part of the leads.

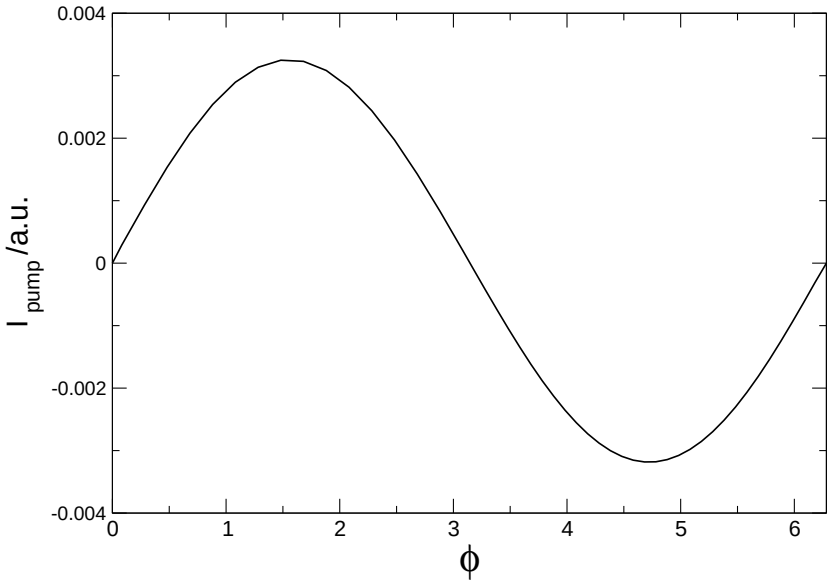

Fig. 15. Parametric pumping through a double square barrier. The device region extends from $x = -6$ to $x = +6$ a.u., the static potential has the value 0.525 a.u. for $5 < |x| < 6$ a.u. and zero elsewhere in the device. Pumping is achieved by harmonic variation of the barriers, i.e., $U(x,t) = U_0 \sin(\omega t)$ for the left barrier (-6 a.u.$< x < -5$ a.u.) and $U(x,t) = U_0 \sin(\omega t + \phi)$ for the right barrier (5 a.u.$< x < 6$ a.u.). The DC component of the pump current is displayed as a function of the phase ϕ. The parameters are: $U_0 = 0.25$ a.u., $\omega = 0.25$ a.u. and the Fermi energy is $\varepsilon_F = 0.5$ a.u..

This implies an effective "metallic screening" of the constriction. The screening limits the spatial extent of the induced density created by the bias potential or the external field to the central region. Our time-dependent scheme allows to extract both AC and DC I/V device characteristics and it is ideally suited to describe external field (photon) assisted processes.

In order to illustrate the performance and potential of the method we have implemented it for one-dimensional model systems and applied it to a variety of transport situations: we have shown that a steady-state current is always reached upon application of a DC bias. For a harmonic AC bias, the resulting AC current need not be harmonic. In the case of systems at DC bias without any source of dissipation it is known that the steady-current is independent of the history of the process[8]. We have explicitly demonstrated this history independence for two different switching processes of the external bias. The history independence for non-interacting electrons not only applies for DC but also for AC bias which we have also demonstrated in a numerical example. Since we can compute current densities locally, we are not restricted to currents deep inside the leads. In one example we have analyzed the time evolution of the density for localized states which are only weakly coupled to the reservoirs. Finally, we have shown a few simple applications of our algorithm to electron pumping.

The list of the example calculations presented here already demonstrates the versatility and flexibility of our algorithm. It includes the Landauer formalism as the long-time limit for systems under DC bias and allows to study transients. Moreover, it can deal with periodic time-dependent fields (which are usually treated with the Floquet formalism) but is applicable to nonperiodic conditions as well [36].

Most theoretical approaches to transport adopt open boundary conditions and assume that transport is ballistic,*i.e.*, under steady state conditions inelastic collisions are absent and dissipation occurs only in the idealized macroscopic reservoirs. This might be an unrealistic assumption for transport through single molecules, in particular when the device is not operated in the regime of small bias and linear response. When inelastic scattering dominates this picture is not applicable. In particular, experiments [37–39] indicate that inelastic scattering with lattice vibrations is present at sufficiently large bias, causing local heating of contacts and molecular devices. In addition, current-induced forces might lead to bond-breaking and electromigrations.

In a joint collaboration with Verdozzi and Almbladh, one of us has included the nuclear degrees of freedom at a classical level[40]. The initial ground state (consisting of bound, resonant and scattering states) has been calculated self-consistently. Also, the time-propagation algorithm of Section 4.2 has been generalized to evolve the system electrons+nuclei in the Ehrenfest approximation. Several aspects of the electron-ion interaction in quantum transport have been investigated.

Electron correlations are also important in molecular conductors, for example, Coulomb blockade effects dominate the transport in quantum dots. Short-range electron correlations seems to be relevant in order to get quantitative description of I/V characteristics in molecular constrictions[41–43]. In particular it is commonly assumed that the energy scales for electron-electron and electron-phonon interactions are different and could be treated separately. However, the metallic screening of the electrodes considerably reduces the Coulomb-charging energy (from eV to meV scale). In this regime the energy scale for the two interactions merge and they need to be treated on the same footing. We would like to emphasize that our scheme allows for a consistent treatment of electronic and ionic degrees of freedom.

It is clear that the quality of the TDDFT functionals is of crucial importance. In particular, exchange and correlation functionals for the non-equilibrium situation are required. Time-dependent linear response theory for DC-steady state has been implemented in Ref. [44] within TDLDA assuming jellium-like electrodes (mimicked by complex absorbing/emitting potentials). It has been shown that the DC-conductance changes considerably from the standard Landauer value. Therefore, a systematic study of the TDDFT function-

als themselves is needed. A step beyond standard adiabatic approximations and exchange-only potentials is to resort to many-body schemes based on perturbative expansions[45,46], iterative schemes[47], or variational-functional formulations[48]. Another path is to explore exchange-correlation functionals that depend implicitly [25,49] or explicitly [50,51] on the current density.

Acknowledgments

This work was supported in part by the Deutsche Forschungsgemeinschaft, by the EU Research and Training Network EXCITING and by the NANOQUANTA Network of Excellence.

References

[1] S. Datta, *Electronic Transport in Mesoscopic Systems* (Cambridge University Press, Cambridge, 1995).

[2] H. Haug and A.-P. Jauho, *Quantum Kinetics in Transport and Optics of Semiconductors* (Springer, Berlin, 1998).

[3] G. Cuniberti, G. Fagas, K. Richter (eds.), *Introducing Molecular Electronics*, Lecture Notes in Physics, Vol. 680 (Springer, Berlin, 2005).

[4] M. Cini, Phys. Rev. B **22**, 5887 (1980).

[5] E. Runge and E. K. U. Gross, Phys. Rev. Lett. **52**, 997 (1984).

[6] G. Stefanucci and C.-O. Almbladh, Europhys. Lett. **67**, 14 (2004).

[7] N. D. Lang, Phys. Rev B **52**, 5335 (1995).

[8] G. Stefanucci and C.-O. Almbladh, Phys. Rev. B **69**, 195318 (2004).

[9] M. Petersilka, U. J. Gossmann and E. K. U. Gross, Phys. Rev. Lett. **76**, 1212 (1996).

[10] S. Kurth, G. Stefanucci, C.-O. Almbladh, A. Rubio and E. K. U. Gross, Phys. Rev. B **72**, 035308 (2005).

[11] L. P. Kadanoff and G. Baym, *Quantum Statistical Mechanics* (Benjamin, New York, 1962).

[12] L. V. Keldysh, JETP **20**, 1018 (1965).

[13] P. Danielewicz, Ann. Physics **152**, 239 (1984) and references therein.

[14] R. Kubo, J. Phys. Soc. Jpn. **12**, 570 (1957).

[15] P. C. Martin and J. Schwinger, Phys. Rev. **155**, 1342 (1959).

[16] R. van Leeuwen, N. E. Dahlen, G. Stefanucci, C.-O. Almbladh, and U. von Barth, *Introduction to the Keldysh Formalism and Applications to Time-Dependent Density Functional Theory*, Lectures Notes in Physics, Springer Verlag, 2006; cond-mat/0506130.

[17] R. van Leeuwen, Phys. Rev. Lett. **80**, 1280 (1998).

[18] P. Hohenberg and W. Kohn, Phys. Rev. **136**, B864 (1964).

[19] N. D. Mermin, Phys. Rev. **137**, A1441 (1965).

[20] M. Di Ventra and T. N. Todorov, J. Phys. C **16**, 8025 (2004).

[21] A. Blandin, A. Nourtier, and D. W. Hone, J. Phys. (Paris) **37**, 369 (1976).

[22] R. Landauer, IBM J. Res. Develop. **1**, 233 (1957).

[23] K. Burke, M. Koentopp, and F. Evers, cond-mat/0502385.

[24] J. R. Hellums and W. R. Frensley, Phys. Rev. B **49**, 2904 (1994).

[25] J.F. Dobson, M.J. Bünner and E.K.U. Gross, Phys. Rev. Lett. **79**, 1905 (1997).

[26] R. van Leeuwen, Phys. Rev. Lett. **82**, 3863 (1999).

[27] N. T. Maitra, K. Burke and C. Woodward, Phys. Rev. Lett. **89**, 023002 (2002).

[28] C. Moyer, Am. J. Phys. **72**, 351 (2004); and references therein.

[29] Higher order propagation schemes could be developed following the ideas discussed here for the modification of the Cayley method. Such schemes could also handle self-consistent and time-dependent Hamiltonians as the ones appearing in standard TDDFT (see A. Castro, M. A. L. Marques and A. Rubio, J. Chem. Phys. **121**, 3425 (2004) and references therein).

[30] H. Appel, L. Wirtz, G. Stefanucci, C.-O. Almbladh, S. Kurth, E. K. U. Gross and A. Rubio (work in progress).

[31] M. Switkes, C.M. Marcus, and A.C. Gossard, Science **283**, 1905 (1999).

[32] P.W. Brouwer, Phys. Rev. B **58**, R10135 (1998).

[33] Y. Wei, J. Wang, and H. Guo, Phys. Rev. B **62**, 9947 (2000).

[34] C.A. Stafford and N.S. Wingreen, Phys. Rev. Lett. **76**, 1916 (1996).

[35] S. Kohler, J. Lehmann, and P. Hänggi, Phys. Rep. **406**, 379 (2005).

[36] X. Oriols, A. Alarcón, and E. Fernàndez-Díaz, Phys. Rev. B **71**, 245322 (2005).

[37] J. G. Kushmerick, J. Lazorcik, C. H. Patterson, R. Shashidhar, D. S. Seferos and G. C. Bazan, Nano Lett. **4**, 639 (2004).

[38] R. H. M. Smit, C. Untiedt and J. M. van Ruitenbeek, Nanotechnology **15**, S472 (2004).

[39] B. J. LeRoy, S. G. Lemay, J. Kong and C. Dekker, Nature **432**, 371 (2004).

[40] C. Verdozzi, G. Stefanucci, and C.-O. Almbladh, cond-mat/0601171.

[41] P. Delaney and J.C. Greer, Phys. Rev. Lett. **93**, 036805 (2004).

[42] F. Evers, F. Weigend and M. Koentopp, Phys. Rev. B **69**, 235411 (2004).

[43] A. Ferretti, A. Calzolari, R. Di Felice, F. Manghi, M. J. Caldas, M. B. Nardelli and E. Molinari, Phys. Rev. Lett. **94**, 116802 (2005).

[44] R. Baer, T. Seideman, S. Ilani and D. Neuhauser, J. Chem. Phys. **120**, 3387 (2004).

[45] A. Marini, R. Del Sole and A. Rubio, Phys. Rev. Lett. **91**, 256402 (2003); L. Reining, V. Olevano, A. Rubio and G. Onida, Phys. Rev. Lett. **88**, 066404 (2002).

[46] I. V. Tokatly and O. Pankratov, Phys. Rev. Lett. **86**, 2078 (2001).

[47] F. Bruneval, F. Sottile, V. Olevano, R. Del Sole, and L. Reining, Phys. Rev. Lett. **94**, 186402 (2005).

[48] U. von Barth, N. E. Dahlen, R. van Leeuwen and G. Stefanucci Phys. Rev. B **72**, 235109 (2005).

[49] Y. Kurzweil and R. Baer J. Chem. Phys. **121**, 8731 (2004).

[50] C. A. Ullrich and G. Vignale, Phys. Rev. B **65**, 245102 (2002); and references therein.

[51] I. V. Tokatly and O. Pankratov, Phys. Rev. B **67**, 201103(R) (2003)